LEVEL II ~ ℓ

(12)

DEVELOPMENT AND VERIFICATION
OF
PYROELECTRIC MATERIALS WITH LOW THERMAL DIFFUSIVITY

FINAL TECHNICAL REPORT
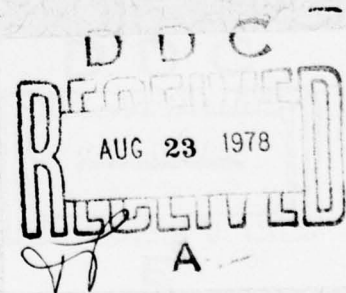15 April 1977 - 15 December 1977


by

G.M. Loiacono
J.P. Dougherty


May 1978


Prepared for

NIGHT VISION & ELECTRO-OPTICS LABORATORIES
USAECOM
Fort Belvoir, Virginia 22060


Contract No. DAAK70-77-C-0098


Prepared by

PHILIPS LABORATORIES
A Division of North American Philips Corporation
Briarcliff Manor, New York 10510

SECURITY CLASSIFICATION OF THIS PAGE (When Data Entered)

| REPORT DOCUMENTATION PAGE | | READ INSTRUCTIONS BEFORE COMPLETING FORM |
|---|---|---|
| 1. REPORT NUMBER | 2. GOVT ACCESSION NO. | 3. RECIPIENT'S CATALOG NUMBER |
| 4. TITLE (and Subtitle)<br><br>DEVELOPMENT AND VERIFICATION OF PYROELECTRIC MATERIALS WITH LOW THERMAL DIFFUSIVITY | | 5. TYPE OF REPORT & PERIOD COVERED<br>Final Technical Report<br>15 April 1977–15 December 1977 |
| | | 6. PERFORMING ORG. REPORT NUMBER |
| 7. AUTHOR(s)<br><br>G.M. Loiacono<br>J.P. Dougherty | | 8. CONTRACT OR GRANT NUMBER(s)<br><br>Contract DAAK70-77-C-0098 |
| 9. PERFORMING ORGANIZATION NAME AND ADDRESS<br><br>PHILIPS LABORATORIES<br>A Division of North American Philips Corp.<br>Briarcliff Manor, New York 10510 | | 10. PROGRAM ELEMENT, PROJECT, TASK AREA & WORK UNIT NUMBERS |
| 11. CONTROLLING OFFICE NAME AND ADDRESS | | 12. REPORT DATE<br>May 1978 |
| | | 13. NUMBER OF PAGES<br>65 |
| 14. MONITORING AGENCY NAME & ADDRESS(if different from Controlling Office)<br><br>Night Vision & Electro-Optics Laboratories<br>USAECOM<br>Fort Belvoir, Virginia 22060 | | 15. SECURITY CLASS. (of this report)<br><br>Unclassified |
| | | 15a. DECLASSIFICATION/DOWNGRADING SCHEDULE |

16. DISTRIBUTION STATEMENT (of this Report)

DISTRIBUTION STATEMENT A
Approved for public release;
Distribution Unlimited

17. DISTRIBUTION STATEMENT (of the abstract entered in Block 20, if different from Report)

DDC
AUG 23 1978
A

18. SUPPLEMENTARY NOTES

19. KEY WORDS (Continue on reverse side if necessary and identify by block number)

pyroelectrics                     figure-of-merit
crystal growth                    triglycine sulfate type crystals
thermal conductivity

20. ABSTRACT (Continue on reverse side if necessary and identify by block number)

The growth of TGS, DTGS, TGFB and DTGFB crystals from solutions containing Cd, Zn, Cu and Pd impurities (5 mole % level) has resulted in improved properties of these pyroelectric materials. Specifically, the optical quality and machinability of Zn and Cd doped crystals improved significantly. The thermal diffusivity and specific heat of the doped crystals were reduced by 10% and 25%, respectively. The effectiveness of the dopants can be classified as Cd>Cu>Zn>Pd. The evidence is clear that metal dopings do effect the thermal properties of these crystals even at the low concentrations incorporated into the host crystals. Further investigations at higher doping levels of both metallic and organic compounds are warranted. Samples of the doped crystals were supplied.

DD FORM 1473 EDITION OF 1 NOV 65 IS OBSOLETE
1 JAN 73

# SUMMARY

The growth of TGS, DTGS, TGFB and DTGFB crystals from solutions containing Cd, Zn, Cu and Pd impurities (5 mole % level) has resulted in improved properties of these pyroelectric materials. Specifically, the optical quality and machinability of Zn and Cd doped crystals improved significantly. The thermal diffusivity and specific heat of the doped crystals were reduced by 10% and 25%, respectively. The effectiveness of the dopants can be classified as Cd>Cu>Zn>Pd. The evidence is clear that metal dopings do effect the thermal properties of these crystals even at the low concentrations incorporated into the host crystals. Further investigations at higher doping levels of both metallic and organic compounds are warranted. Samples of the doped crystals were supplied.

3

## PREFACE

This work was performed by Philips Laboratories, a Division of North American Philips Corporation, Briarcliff Manor, New York, under the overall supervision of Dr. S.K. Kurtz, Director, Exploratory Research Group. Mr. G.M. Loiacono, Senior Program Leader for Crystal Growth and Materials Technology, was the Program Leader and directed the crystal growth effort. Dr. J.P. Dougherty, Materials Scientist, was responsible for the electrical measurements. Dr. E.H. Stupp, Senior Program Leader, Component and Device Research Group, consulted on device considerations of the materials studied.

The program was issued by the U.S. Army Mobility Equipment Research and Development Center, Fort Belvoir, Virginia, and was initiated under Contract DAAK70-77-C-0098. Dr. E.J. Sharp was the Contracting Officers' Representative for the Night Vision & Electro-Optics Laboratories, USAECOM.

The work described in this Final Technical Report covers the period from 15 April 1977 to 15 December 1977.

# TABLE OF CONTENTS

# LIST OF ILLUSTRATIONS

Page

## LIST OF ILLUSTRATIONS (Cont'd)

# LIST OF TABLES

# 1.    INTRODUCTION

The objective of this research program was the development and experimental verification of materials having low thermal diffusivity without degradation of the pyroelectric response characteristics.

In a thermal imaging system using a pyroelectric vidicon, the rate at which the generated image spreads (i.e., loss of resolution) depends inversely on the thermal diffusivity (k) of the target material.  It is obvious that a low thermal diffusivity imparts directly on the performance of the thermal imaging system.  Previous studies have shown that the thermal diffusivity of triglycine sulfate (TGS) can be modified by impurity additions and growth techniques (Refs. 1-4).  A recent study has shown that deuteration of triglycine fluoroberyllate (TGFB) also effects thermal diffusivity (Ref. 5).  This data is listed in Table 1.

TABLE 1.  THERMAL DIFFUSIVITY (k) AND CURIE TEMPERATURE OF PYROELECTRIC MATERIALS.

| Crystal | Curie Temp. ($^\circ$C) | Thermal Diffusivity $(cm^2/s) \times 10^{-3}$ |
|---------|------------|-----------------------|
| TGS     | 49 | 2.8 |
| TGFB-1  | 73 | 2.0 |
| TGFB-2  | 73 | 2.1 |
| DTGFB-2 | 75 | 1.7 |
| DTGFB-2 | 82 | 3.0 |
| DTGFB-1 | 83 | 2.4 |

The designation TGFB-1 and TGFB-2 means that these samples were obtained from different sources.  It is apparent that the thermal diffusivity of TGFB is 25% lower than the standard TGS target, both materials being undoped.  The scatter of values for k of the DTGFB samples is probably related to the history of the sample (i.e., defect structure) and it is interesting to note the 40% lower value for DTGFB ($T_c$ = 75°C).  This sample was

known to contain a high density of crystalline defects such as dislocations and confirms previously reported data on thermal diffusivity (Ref. 2). It is also known that changes in domain wall density and configuration have significant effects on thermal diffusivity, and that both crystal growth conditions and purity affect domains. For example, the incorporation of an impurity could result in a crystalline defect (high dislocation area) thereby pinning the domain wall. In addition, recent work with metal-doped TGS has produced crystals with shorter phonon mean-free paths, thereby resulting in lower thermal diffusivity.

While it is not clear what effect the presence of impurities would have on thermal diffusivity in a defect-free crystal, the generation of defects by the impurity could be assumed to contribute to the total reduction of thermal diffusivity.

The use of metal impurity doping of TGS and related materials has demonstrated additional effects on dielectric constant ($\varepsilon$), pyroelectric coefficient ($\pi$), and ferroelectric Curie temperature ($T_c$) [Refs. 6-10]. Of special interest was the observation that uniformity of impurity incorporation in TGS had dramatic effects on dielectric constant and pyroelectric coefficient (Ref. 10). These effects were directly related to the crystal growth conditions (i.e., static vs. dynamic) for TGS doped with Cd and Mn ions and are illustrated in Table 2.

TABLE 2. EFFECTS OF METAL IONS IN TGS (at 35°C).

| Metal Ion | Pyroelectric Coefficient ($\mu C \times 10^{-2} \cdot cm^{-2} \cdot K^{-1}$) | Dielectric Constant |
|---|---|---|
| Cd (Static) | 5.9 | 345 |
| (Dynamic) | 5.0 | 67 |
| Zn (Static) | 5.8 | 1000 |
| (Dynamic) | 4.7 | 80 |

Impurity doping of TGS has shown that a significant improvement in pyroelectric vidicon performance is attainable, and indicated a similar study of DTGS, TGFB and DTGFB could result in further improvements.

The goal of this program was to further exploit the work identified above so as to provide pyroelectric target materials with a reduction in thermal diffusivity of at least 50% over that of pure TGS, without increasing the dielectric constant nor decreasing the pyroelectric coefficient of the host crystal. In particular, TGS, DTGS, TGFB and DTGFB crystals both pure and doped would be grown and their relevent properties measured.

## 2.    EXPERIMENTAL

### 2.1    Crystal Growth of TGS, DTGS, TGFB and DTGFB

### 2.1.1    Preparation of Solutions

The synthesis of TGS was performed according to the reaction:

$$3NH_2CH_2COOH + H_2SO_4 \xrightarrow[70°C]{H_2O} (NH_2CH_2COOH)_3 \cdot H_2SO_4 \qquad (1)$$
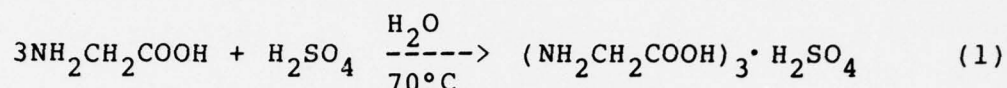
After the reaction was completed, the solution was slowly cooled to room temperature and the crystallized TGS collected for subsequent preparation of growth solutions. In the case of TGFB, a new synthesis procedure developed prior to this program was employed. The synthesis is described by the reactions:

$$Be + 4 HF \xrightarrow[10°C]{H_2O} H_2BeF_4 + H_2 \uparrow \qquad (2)$$

$$H_2BeF_4 + 3NH_2CH_2COOH \xrightarrow[70°C]{H_2O} (NH_2CH_2COOH)_3 \cdot H_2BeF_4 \qquad (3)$$
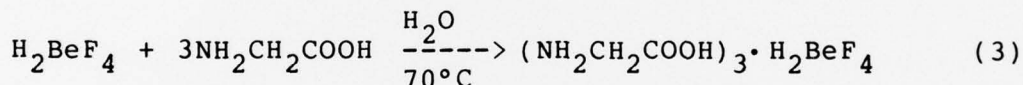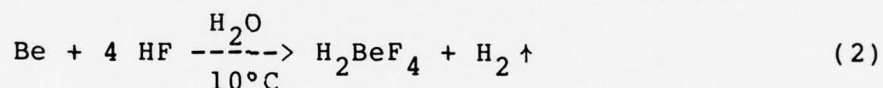
The initial reaction (Eq. 2) of metallic Be with HF is highly exothermic (~90 Kcal/mole) and it is necessary to use a constant temperature bath held at 10°C. HF is added slowly over a ten hour period. It was observed that the first reaction (Eq. 2) is actually a two step process, in which the intermediate compound $BeF_2$ is formed and subsequently converted to $H_2BeF_4$. After the last reaction (Eq. 3), crystalline TGFB is obtained by cooling the solution to 10°C. This material is subsequently used to prepare growth solutions. One of the advantages of using metallic Be instead of the carbonate or hydroxide compounds is the reduction of the health hazard involved in handling Be compounds in powder form. The most important advantages are the strict control of stoichiometery by use of

14

metallic Be and the high resulting purity. The commercially available carbonate and hydroxide are known to contain up to 0.1% impurities and/or other Be compounds and, in addition, are extremely hydroscopic which causes problems in handling. Table 3 lists the purity of the starting components used in this program and their sources. The purity of the dopants used to produce crystals with specific metallic impurities were all in the range of 99+% (Reagent Grade).

TABLE 3. PURITY OF STARTING MATERIALS.

| Impurity | HF(48%)[a] | $H_2SO_4$[b] | Be[c] | Glycine[d] |
|---|---|---|---|---|
| | Concentration (ppm) | | | |
| Al | 0.05 | 0.01 | 30 | -- |
| B | -- | -- | 1 | -- |
| Ca | -- | -- | 20 | -- |
| Cr | 0.5 | -- | 5 | -- |
| Cu | 0.1 | 0.1 | 10 | -- |
| Fe | 0.5 | 0.2 | 25 | 10 |
| Mg | 0.2 | -- | 20 | -- |
| Mn | -- | -- | 10 | -- |
| Ni | 0.1 | -- | 30 | -- |
| Si | 0.5 | 0.5 | 25 | -- |
| Pb | 0.1 | 1.0 | -- | 10 |
| Zn | -- | -- | 30 | -- |

(a) HF(48%) Mallinckrodt Transit AR Grade.
(b) $H_2SO_4$ Mallinckrodt Transit AR Grade.
(c) Be Atomergic Grade AA (99.9+%).
(d) Glycine MCB High Purity 99% $NH_3$ Free.

The preparation of the corresponding deuterated compounds DTGS and DTGFB were performed by dissolving the appropriate salt in 99.9+% $D_2O$. The resulting growth solutions were nominally saturated at 40°C and crystals grown from these solutions had deuterium concentrations as shown in Table 4. The deuteration level of the DTGS crystals were inferred to be ~ 90%, from a comparison of their ferroelectric Curie temperatures with pure DTGS:95%D given in Table 5. Deuteration of TGS and TGFB has a significant effect on both electrical and physical properties of

15

TABLE 4.  DEUTERIUM CONCENTRATION IN
DTGFB CRYSTALS.

| Crystal | [D] $\pm$ 2% |
|---------|--------------|
| DTGFB:Cu | 70 |
| DTGFB:Zn | 67 |
| DTGFB:Cd | 66 |
| DTGFB:Pd | 62 |

TABLE 5.  EFFECTS OF DEUTERATION IN TGS AND TGFB[11]

| Crystal | [D] (%) | $T_c$ (°C) | Curie Constant (°K) | Pyroelectric[a] Coefficient ($\mu$Cx$10^{-2}$.cm$^{-2}$.K$^{-1}$) | Dielectric[b] Constant |
|---------|---------|------------|---------------------|------------------------------------------------------------------|------------------------|
| TGS | 0 | 49.0 | 3780 | 4.13 | 77 |
| DTGS | 95 | 61.1 | 2670 | 3.26 | 25 |
| TGFB | 0 | 73.8 | 2660 | 2.39 | 24 |
| DTGFB | 70 | 74.7 | 2190 | 3.21 | 17 |

(a) and (b) measured at 35°C.

these crystals.  Table 5 gives a comparison of both forms of TGS
and TGFB.  It is clear that deuteration increases $T_c$ and
causes a significant decrease in dielectric constant (Ref.
11).

2.1.2   Dopant Additions

Based on data previously published, the impurities selected for
investigation were Cu, Zn, Cd and Pd (Refs. 4,6,7,9,12,13).  The
effects of Zn and Cd doping of TGS have been discussed in
Section 1.  The effects of Pd doping in TGS are a large increase
in crystal growth rate, and a marked effect on domain structure
(Ref. 9).  Strong internal bias fields (4.9 kV/cm) in TGS are
developed by Pd doping coupled with a decrease in maximum
dielectric constant (6.5 x $10^4$ down to 3.1 x $10^3$).  In the
case of Cu doped TGS, and TGFB similar results were reported
(Refs. 4,7,13).

16

The four host crystals; TGS, DTGS, TGFB and DTGFB were each grown with Cu, Zn, Cd and Pd dopants. The initial dopant concentration in the growth solution was about 5 mole % based on the moles of solute present at the saturation temperatures selected.

### 2.1.3   Crystallizers

A new type solution growth crystallizer was used for this program. The main advantages of this unit are; four separate growth chambers, identical rotation rate, identical temperature programming rates and finally four growth runs can be completed within the time required for one single experiment using the standard crystallizers. Figure 1 illustrates this apparatus.
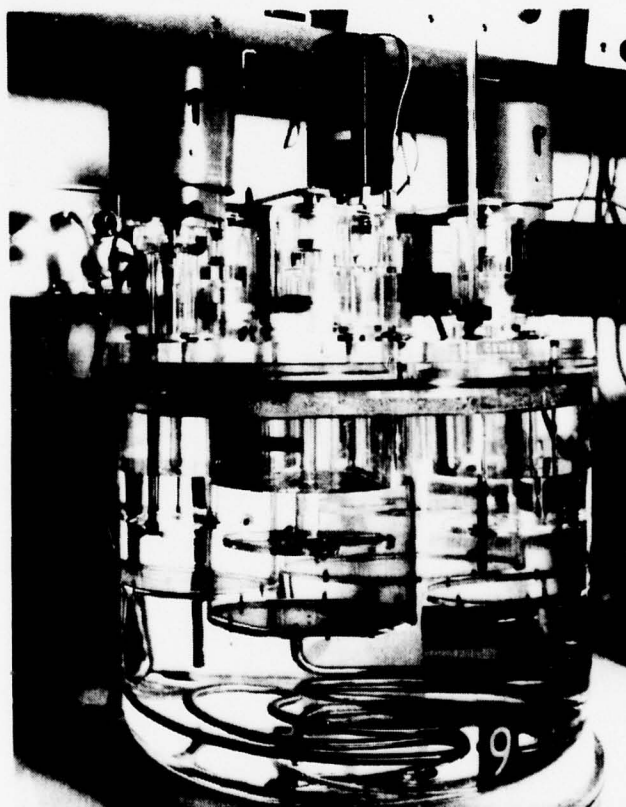


Figure 1.   Multi-chamber solution growth crystallizer.

The temperature control of this system is stable to $\pm$ 0.005°C. Four complete sets of identical seed holders are used and all seed crystals are mounted at the same distance from the center of rotation. This permits, using a single rotation speed, identical solution velocities to flow against the growing seed crystal. The growth chambers were constructed of glass (TGS growth) or Lucite (TGFB growth).

### 2.1.4   Crystal Growth

Saturation Temperature.   All growth solutions were initially saturated at approximately 40°C. The saturated solutions were allowed to equilibrate for 96 hours in the presence of excess solute. After equilibration, the solutions were decanted into holding tanks and the temperature increased to 60°C. The solutions were held at 50°C for 24 hours and then filtered through a 0.4 $\mu$m millipore filter system. The filtered solutions were then allowed to cool to within 2°C of their saturation temperatures and loaded directly into the pre-equilibrated growth chambers containing the seed crystals.

Seed Crystals.   The majority of seed crystals used for growth were cylindrical ~15-20 mm dia. by 3 mm thick. In some experiments flat rectangular seed plates were employed. All seed crystals had the [010] crystallographic orientation perpendicular to the plate surface. Figure 2 illustrates a typical seed holder and the location of the seed crystals. Figure 3 illustrates another seed holder arrangement used, which featured holding the seed crystal in an O-ring. Crystals therefore grew from both sides of the seed as shown.
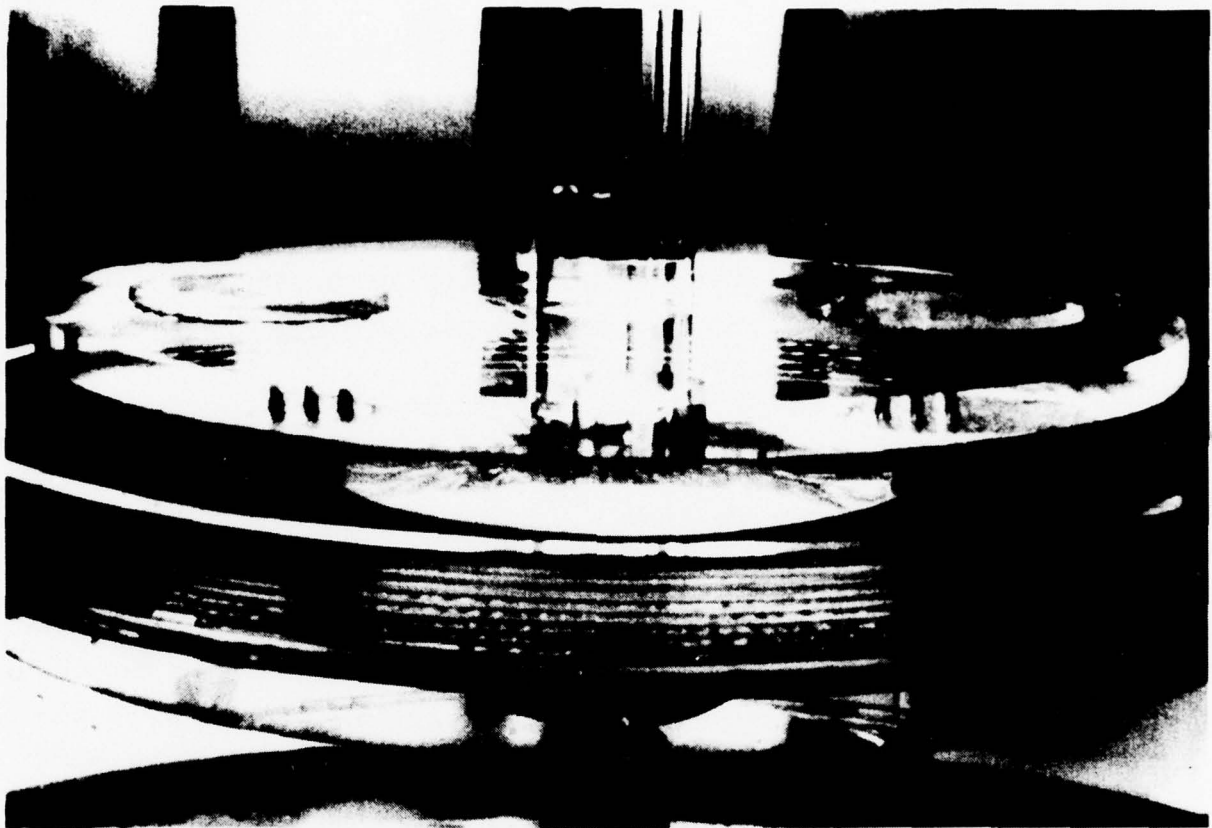
Figure 2. Typical seed holder configuration (cylindrical seeds).



Figure 3. O-ring type seed holder (TGFB-Zn 9-215).

Crystal Growth Parameters.  The solution volumes used for the various compositions grown were in the range 1.4 to 2.0 liters. Seed rotation rates were fixed at 20 rpm (effective solution velocity 7 cm/s).  One run 9-215, had a rotation rate of 60 rpm. The temperature lowering rate was initially 0.05°C/day, which was increased to 0.1°C/day linearly over a 15 day period and then held constant at 0.1°C/day.

## 2.2     Characterization and Property Measurements

### 2.2.1    Density Determinations

The density of both pure and doped samples of all crystals was measured by Archimedes Principle.  The values are estimated to be $\pm$ 0.008.  In regard to the effect of temperature on the density of these materials, previous data clearly shows that the density of TGFB does not change significantly from 25° to 80°C (1.64 to 1.63 g/cm$^3$) (Ref. 14).

### 2.2.2    Dopant Concentrations

The concentrations of dopants in both the growth solutions and crystals were determined using atomic absorption spectrophotometry by the Spectrochemical Corporation of Franklin Lakes, N.J.  The crystalline samples were dissolved in distilled water in order to eliminate variations due to non-uniform impurity distributions.  Therefore, the reported values are average concentrations.

### 2.2.3    Specific Heat

Specific heat measurements were performed with a Perkin Elmer differential scanning calorimeter (Model DSC-2) capable of operating over the temperature range -175°C to +725°C.  The instrument was calibrated with both a pure indium standard (M.P. 429.78°K) and single crystal sapphire for Cp measurements.  The specific heat of each sample was measured from room temperature

through their respective Curie temperatures at a constant heating rate of 10°/min. Sample size ranged from 10 to 30 mg. All measurements were made in air.

### 2.2.4 Thermal Conductivity

Thermal conductivity measurements were made with a TC-100 twin standard thermal conductivity instrument manufactured by Sparrell Engineering Corp. of Salem, Mass. The instrument utilizes a comparison method for determination of thermal conductivity. A sample of the unknown material is sandwiched between two identical standards made from Corning Pyrex 7740 glass. A comparison between the thermal gradients (under equilibrium conditions) in the known and unknown crystals, permits the thermal conductivity of the unknown to be determined.

The heat flux through any of the three stack components is given by:

$$\frac{Q}{A} = \frac{K\Delta T}{\Delta X} \qquad (4)$$

where K is the thermal conductivity, T the temperature (°C) and X the sample path length (cm). If the radial heat losses are small, or uniform down the stack, the average flux passing through the two standard components can be taken as equal to the flux through the sample.

The average temperature drop across the two standards and the sample are determined from the thermocouple outputs. The average standard thermal conductivity is then obtained from a standard curve corresponding to the variation of K with temperature for Pyrex 7740. Knowing the thickness ($\Delta X$) of the sample and of the standards, the ratio of temperature drops across each stack, and the thermal conductivity of the standard, the thermal conductivity of the sample can be calculated from:

21

$$K_{sample} = K_{stds.} \left( \frac{\Delta T_{std.}}{\Delta T_{sample}} \right) \left( \frac{\Delta X_{sample}}{\Delta X_{std.}} \right) \tag{5}$$

The samples used for thermal conductivity measurements were prepared, from each crystal grown, in the form of rods having a diameter $15 \pm 0.01$ mm and lengths as long as possible (> 10 mm). In order to conserve time and crystalline material, a preliminary study was made of pure TGS in three crystallographic orientations; [100], [010] and [001]. Based on the results of these experiments, the other pure and doped crystals were all fabricated with the rod axis parallel to the [010].

Each measurement of a data point required about 18 hours to attain equilibrium conditions.

### 2.2.5    Thermal Diffusivity

The thermal diffusivity (k) of the pure and doped crystals was calculated from the relationship:

$$k = \frac{K}{C_p \rho} \quad (cm^2/s) \tag{6}$$

where K is the thermal conductivity, $C_p$ the specific heat and $\rho$ the density of the sample.

### 2.2.6    Dielectric Constant

Samples for all electrical measurements were cut and polished to thicknesses of 350 to 700 $\mu$m. The electrode area always covered the entire sample surface. In addition, the aspect ratios of sample diameter to thickness was always > 10 allowing the use of the parallel plate approximation for capacitance.

Samples were electroded with either evaporated gold or air drying silver paste. When properly poled the dielectric and pyroelectric properties showed no measureable difference as a function of electrode material. Silver paste contacts were used on the majority of samples as a matter of convenience.

22

In order to properly characterize the dielectric constant of a
pyroelectric material with respect to the material's usefulness
as a vidicon target several measurement parameters must be
considered. These are:

- Poling state of the sample.
- Magnitude and frequency of the small signal
  measuring field.
- dc bias fields.

Domain wall contribution to the measured capacitance of TGS,
TGFB type materials appears to be significant. Capacitance
values of samples in the electrically depoled state (after a
hysteresis loop) reduced by as much as a factor of 10 after
being poled.

Therefore, to satisfy condition one adequately, the crystal
should be poled until no further changes in capacitance are
observed. On removal of the poling field it should further be
verified that no depoling occurs. Poling was accomplished and
verified on all of our samples before the dielectric constant
was measured. The magnitude of the small signal measuring field
should be low in order that domain wall motion does not con-
tribute to the measured capacitance. We have observed that
fields as low as 0.06 kV/cm at 60 Hz can produce a ferroelectric
hysteresis loop. Dielectric constants measured under these
conditions will show an anomalously high value of $\varepsilon$; twofold
increases are not uncommon.

We measured capacitance with a Boonton capacitance meter. The
test signal for this instrument was 100 mV compared to 500 mV or
1 V typical of many capacitance bridges. The frequency of our
test signal was 1 MHz. The higher frequency will tend to
inhibit domain wall motion since coercive fields increase with
frequency. The dielectric constant at 1 MHz is very close to
the 5 MHz value which is most characteristic of the dielectric
constant involved in the beam read-out efficiency of a vidicon

target. The dielectric constant related to the production of the pyroelectric signal as a low frequency value (< 10 Hz). This low frequency $\varepsilon$ can be most suitably found by dynamic techniques (Chynoweth). However, absolute calibration of Chynoweth techniques is very difficult.

Pyroelectric vidicons are operated with a bias field on the target. We have therefore applied a dc bias field (typically 0.5 kV/cm) to the sample as the capacitance is being measured. The bias field has the further advantage of preventing depoling due to thermal fluctuations or the ac test voltage.

It is clear from the above discussion that our measurements of dielectric constant were performed under different boundary conditions than those typically reported in the literature. Most reported values of $\varepsilon$ were derived from data collected on poled, but unbiased, samples at a frequency of 1 kHz with test voltages usually a factor of 5 larger than ours. We would expect the different test conditions to manifest themselves largest near $T_c$ where the coercive field is approaching zero and electrostrictive effects of bias voltages are greatest. This has been confirmed by our observations.

### 2.2.7  Pyroelectric Coefficients

The pyroelectric coefficient, p, is the rate of change of the spontaneous polarization, $P_s$, with temperature, T:

$$p = \frac{d P_s}{dT} = \frac{d P_s}{dt} \frac{dt}{dT} = \frac{I_p}{A \, (dT/dt)} \tag{7}$$

where $I_p$ is the pyroelectric current, A is the electrode area, and dT/dt is the heating or cooling rate. When a linear heating rate is used to find p, the technique is called the Byer-Roundy method.

We have used the Byer-Roundy technique to measure p; where dT/dt was observed to deviate from linearity, the exact value of

24

dT/dt was explicity calculated. The runs were performed on cooling from above the Curie temperature, $T_c$ with a poling field applied and maintained in order to prevent depoling. Contributions to $I_p$ from conductivity were usually negligible.

An independent cross-check of the pyroelectric coefficients was performed. The values of $I_p$ were integrated from $T_c$ to room temperature and compared to the spontaneous charge measured by a Sawyer-Tower circuit. Calculation of $P_s$ by the two methods agreed to within 10%.

### 2.2.8   Hysteresis Loops

Ferroelectric hysteresis loops were measured using a modified Sawyer-Tower circuit. From these loops, $P_s$ and coercive field, $\varepsilon_c$ were determined. Since the hysteresis loops showed flat saturation arms with no opening near the peak voltages, it was not necessary to compensate the effects of linear capacitance or conductance on the measured charge-voltage characteristics.

3.        RESULTS AND DISCUSSION

3.1       Crystal Growth

A total of 24 crystal growth runs were completed during this program. A summary of the crystal growth is presented in Table 6. The grown boules were typically in the 20 to 80 g range and in most cases were free from macroscopic defects (i.e., cracks). Figures 4, 5 and 6 illustrate doped grown boules of DTGS, DTGFB and TGFB. In the case of Zn doped TGFB and DTGFB, a pronounced reduction in the susceptibility of the crystal's surface to hydrolyze was observed. The deuterium content of the DTGFB crystals was given in Table 4. The deuterium levels of the DTGS crystals are estimated to be similar to those measured in the DTGFB.

There were two significant problems in the growth phase of this program. First, the amount of spurious nucleation (see Table 6) produced during the majority of the TGFB and DTGFB growth runs caused severe variations in crystal growth rate. This in turn contributed to the non-uniform distribution of dopant in the grown crystal. This problem can be eliminated by selection of a post-saturation treatment of the growth solution. We have recently demonstrated that a DTGFB saturated solution, treated at 60°C for 24 hours, had no observable spurious nucleation after one month of growth. Non-uniform distribution of dopant was the other growth problem. While inhomogenity of dopants was easily observed in Cu and Pd doped crystals, the Zn and Cd samples were colorless. In general preferential incorporation of the colored ions was localized in the (110) growth sectors. Figure 7 clearly illustrates this effect in Pd doped TGS. To obtain a completely uniform doping in the TGS crystals will require additional effort in assessment of the effects of initial dopant concentration, pH, growth rate and seed orientation.

We feel that neither of the above problems are critical.

## TABLE 6. SUMMARY OF CRYSTAL GROWTH DATA.

| Run No. | Composition | Saturation Temp. (°C) | pH @ 20°C | $\Delta T$ (°C) | Crystal Yield (g) | Spurious (g) | Deposition Rate (g/ℓ/°C) |
|---|---|---|---|---|---|---|---|
| 9-189 | TGS:Cd | 40.3 | 2.21 | 4.60 | 56.7 | 0 | 8.4 |
| 9-189 | TGS:Zn | 40.7 | 2.25 | 4.60 | 57.4 | 1.0 | 8.3 |
| 9-189 | TGS:Cu | 40.3 | 2.22 | ---------------Aborted--------------- | | | |
| 10-193 | TGS:Cu | 40.2 | 2.17 | 6.41 | 65.9 | 2.6 | 7.2 |
| 9-205 | TGS:Pd | 40.7 | 2.03 | 1.72 | 28.7 | 0 | 11.9 |
| 9-215* | TGS:Pd | 40.3 | 2.03 | 5.74 | 23.4 | 0 | 2.9 |
| 10-193 | DTGS:Cd | 40.4 | 2.17 | 6.41 | 76.8 | 6.0 | 8.8 |
| 9-205 | DTGS:Cd | 40.7 | 2.22 | 1.72 | 20.0 | 35.0 | 19.9 |
| 9-215* | DTGS:Cd | 40.3 | 2.22 | 5.74 | 52.1 | 0.9 | 6.6 |
| 9-189 | DTGS:Cu | 40.3 | 2.22 | 4.60 | 31.5 | 0 | 4.7 |
| 10-193 | DTGS:Cu | 40.3 | 2.20 | 6.41 | 79.3 | 10.1 | 9.7 |
| 10-193 | DTGS:Zn | 40.6 | 2.21 | 6.41 | 81.4 | 4.2 | 9.2 |
| 9-205 | DTGS:Pd | 40.7 | 2.07 | 1.72 | 21.3 | 0 | 8.2 |
| 9-215* | DTGS:Pd | 40.3 | 2.07 | 5.74 | 24.0 | 0.6 | 3.1 |
| 10-201 | TGFB:Cd | 37.5 | 2.3 | 4.42 | 50.0 | 28.5 | 11.8 |
| 10-201 | TGFB:Cu | 37.4 | 2.3 | 4.42 | 24.3 | 28.5 | 7.9 |
| 10-201 | TGFB:Pd | 37.5 | 2.2 | 4.42 | 34.3 | 28.0 | 9.4 |
| 10-201 | TGFB:Zn | 37.5 | 2.3 | ---------------Aborted--------------- | | | |
| 9-205 | TGFB:Zn | 40.7 | 2.3 | 1.72 | 30.5 | 21.0 | 18.6 |
| 9-215* | TGFB:Zn | 40.3 | 2.3 | 5.74 | 44.1 | 24.2 | 8.5 |
| 9-194 | DTGFB:Cu | 40.5 | 2.0 | 6.04 | 72.1 | 53.0 | 14.7 |
| 9-194 | DTGFB:Cd | 40.5 | 2.4 | 6.04 | 67.4 | 43.4 | 13.0 |
| 9-194 | DTGFB:Zn | 40.4 | 1.9 | 6.04 | 84.2 | 21.2 | 12.5 |
| 9-194 | DTGFB:Pd | 40.5 | 2.3 | 6.04 | 72.9 | 24.3 | 11.5 |

* Run No. 9-215 new type seed holder.

27

(a) Side view.



(b) Top view.

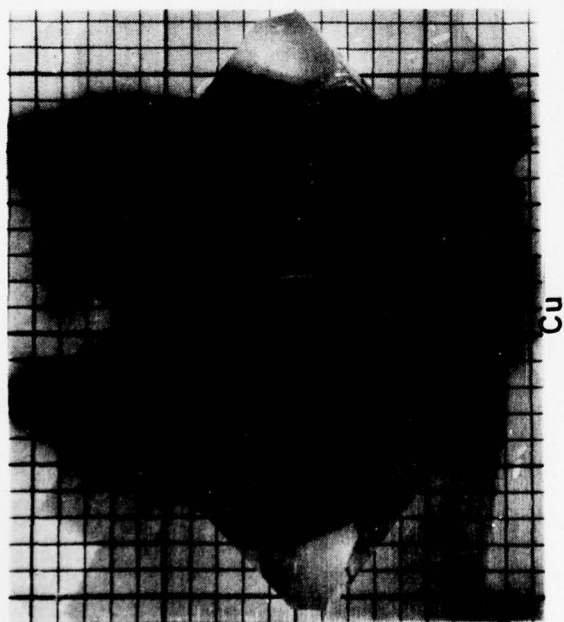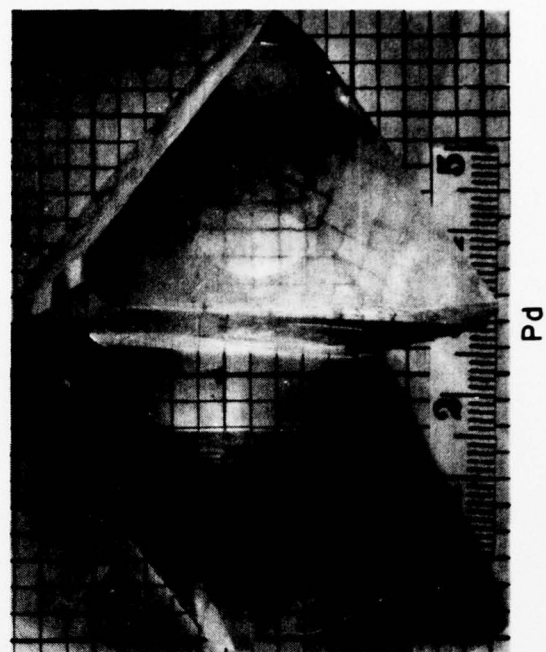Figure 4.   Grown crystals of DTGS:Cd (9-215).
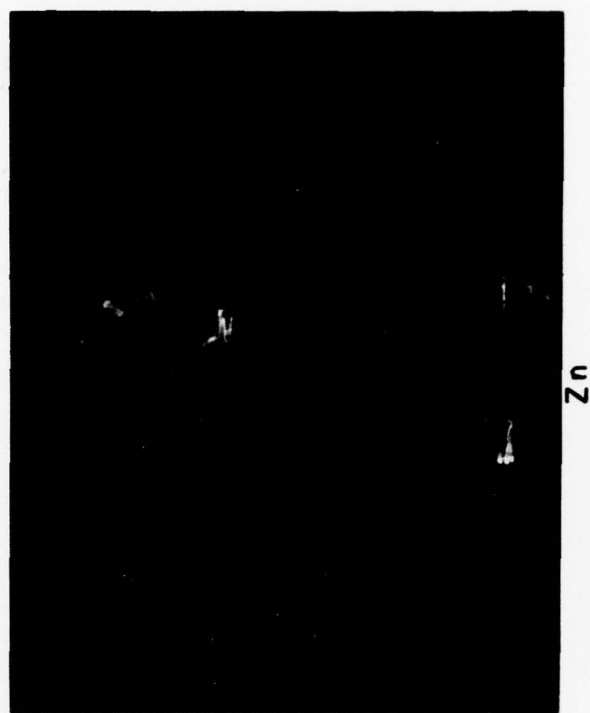
Figure 5. DTGFB crystals (9-194).

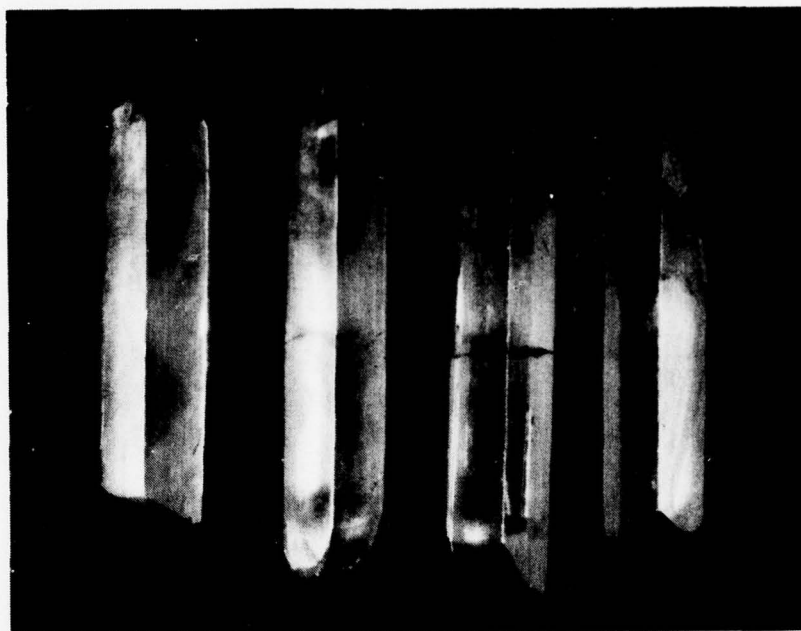Figure 6. TGFB crystals (10-201 and 9-215).

Figure 7.  Dopant banding in TGS:Pd.

A number of interesting dopant effects were observed in this program.  The growth rate, and subsequent optical quality of all host crystals was improved when Zn and Cd were used as dopants. In particular, Zn doped TGFB grew extremely well and subsequently, during fabrication of the boules into rods and slices, we noted marked differences (improvement) in the machinability of this material.  The same general behavior was observed for Cd doped crystals.

The external morphology (crystal habit) of the doped crystals are illustrated in Figures 8-11.  A strong morphological distortion was observed for Pd doped TGS and DTGS where growth was predominately in the [001].  Qualitatively, the number of facets in TGS and DTGS decrease with dopants, while for TGFB and DTGFB the number remain about constant (see Table 7).  The largest change is observed for Pd doping of TGS and DTGS.

The metal dopant concentrations for both growth solution and crystal are listed in Table 8.  Included in this table is the
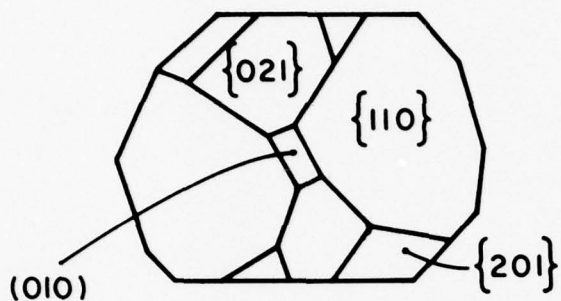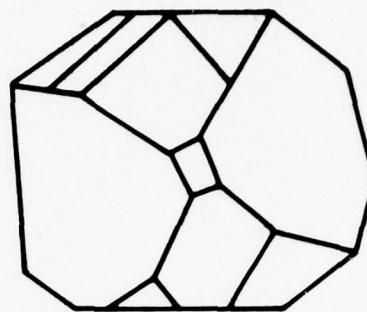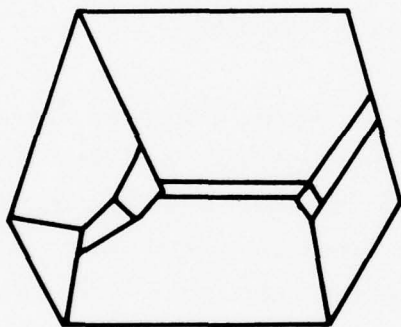
Figure 8.   Morphology of doped TGS crystals.

{021}   {201}

(010)

{110}
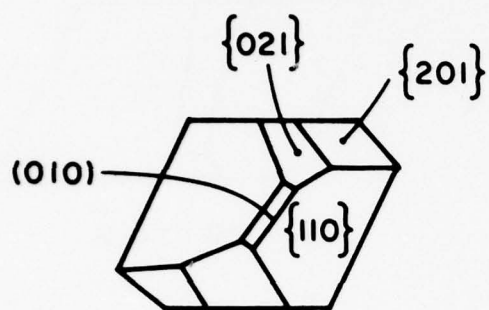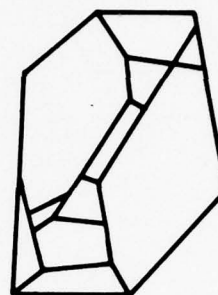
DTGS: Cu

DTGS: Zn
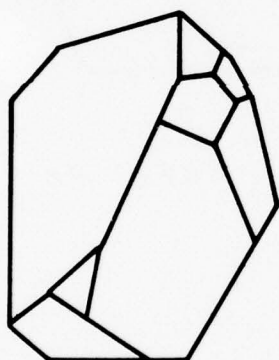
DTGS: Cd

DTGS: Pd

Figure 9.  Morphology of doped DTGS crystals.

33

a) TGFB : Zn   TOP

b)   BOTTOM

{110}

(010)

(021)
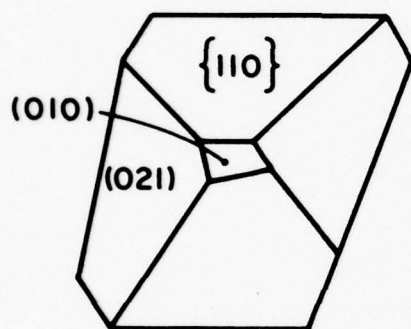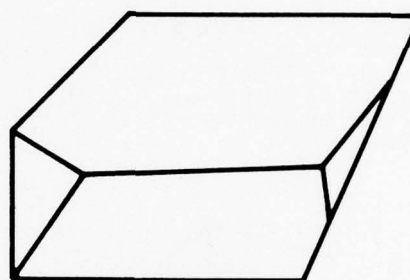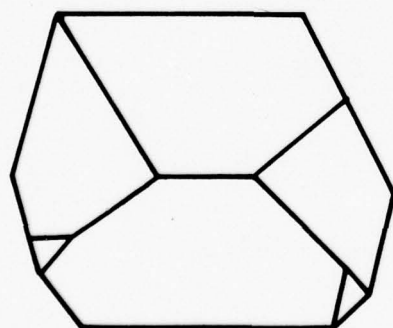
c)   TGFB : Cd

d)   TGFB : Pd

Figure 10.   Morphology of
doped TGFB crystals.

e)   TGFB : Cu

34
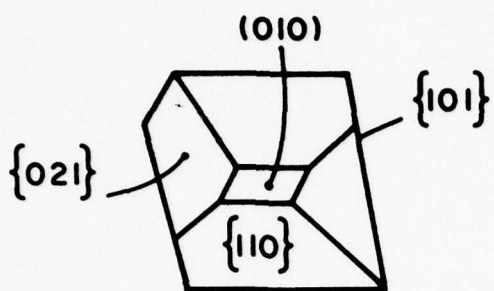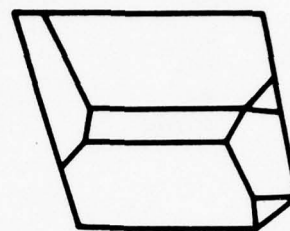
a). DTGFB: Cu    b) DTGFB: Cd
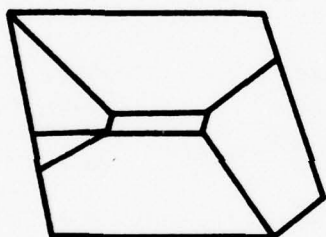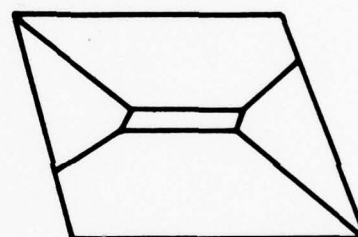
c) DTGFB: Zn    d) DTGFB: Pd

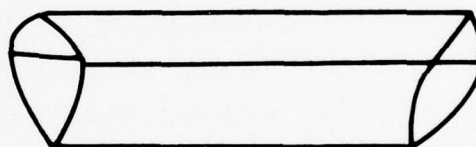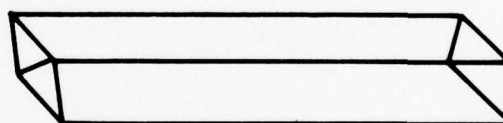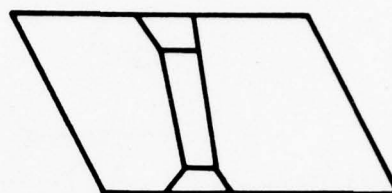Figure 11.  Morphology of doped DTGFB crystals.

TABLE 7.   MORPHOLOGY VARIATIONS.

| | --------Number of Facets------- | | | |
| Dopant | TGS | DTGS | TGFB | DTGFB |
|--------|-----|------|------|-------|
| Cu: | 10 | 7 | 6 | 5 |
| Zn: | 10 | 11 | 3 | 6 |
| Cd: | 9 | 8 | 5 | 7 |
| Pd: | 6 | 6 | 4 | 5 |
| Pure: | 19 | 19 | 4 | 4 |

TABLE 8.   METAL DOPANT CONCENTRATIONS.

| | | --Concentration(ppm)-- | | |
| Crystal | Metal | Solution | Crystal | $k_{eff} \times 10^{-3}$ |
|---------|-------|----------|---------|------------------|
| TGS | Cu | 2350 | 35 | 15.0 |
| | Zn | 3650 | 10 | 3.0 |
| | Cd | 2900 | 1 | 0.3 |
| | Pd | -- | -- | ---- |
| DTGS | Cu | 2900 | 20 | 7.0 |
| | Zn | 3750 | 15 | 4.0 |
| | Cd | 3850 | 0.3 | 0.078 |
| | Pd | 4250 | 60 | 14.0 |
| TGFB | Cu | 4400 | 30 | 6.8 |
| | Zn | 5150 | 3 | 0.58 |
| | Cd | 5900 | 1.5 | 0.25 |
| | Pd | 4100 | 90 | 22.0 |
| DTGFB | Cu | 4450 | 30 | 6.7 |
| | Zn | 5950 | 5 | 0.84 |
| | Cd | 9200 | 25 | 2.7 |
| | Pd | 230 | 10 | 43.0 |

average effective distribution coefficient of the metal which is the ratio of metal concentration in the crystal to that in solution:

$$k_{eff} = \frac{[M]_C}{[M]_S} \tag{8}$$

The $k_{eff}$ values are quite small and vary in some cases for a single metal in a similar crystal host (i.e., $10^{-2}$ Cu·TGS and $10^{-3}$ Cu·DTGS). This behavior can be attributed to differences

36

in growth rate, which in the case of these Cu doped samples varied by a factor of two. In addition the observed non-uniform distribution of dopant would contribute an error to the actual metal content contained in the crystal used for analysis. The $k_{eff}$ values given in Table 8 should only be used on a qualitative basis in further dopant studies.

## 3.2    Density

The density of the pure and doped crystals were measured using Archimedes Principle and are good to $\pm$ 0.008. Table 9 lists the measured values. There are no significant effects on the pure crystal density except possibly in the case of Cu doped TGFB. There is an appreciable increase in density upon deuteration of TGFB which was expected. These values are used for subsequent figure-of-merit calculations in Section 3.5.

TABLE 9.    DENSITIES OF TGS TYPE CRYSTALS ($\pm$ 0.008) (at 25°C).

| Crystal | Pure | Zn | Cd | Cu | Pd |
|---------|------|------|------|------|------|
| DTGFB | 1.660 | 1.664 | 1.669 | 1.671 | 1.672 |
| TGFB | 1.628 | --- | 1.631 | 1.617 | 1.625 |
| TGS | 1.663 | 1.665 | 1.670 | 1.665 | --- |
| DTGS | --- | 1.717 | --- | 1.717 | --- |

## 3.3    Specific Heat Data

The specific heat measurements on pure TGS, DTGS and DTGFB are shown in Figure 12. The difference in $C_p$ at 313°K between TGS and DTGS is only 3%. Comparison of $C_p$ for DTGFB and TGS indicates that DTGFB is about 22% higher. The comparison is made at 313°K and 335°K which represents the actual PEV operating temperatures for TGS and DTGFB, respectively. It can be seen that deuteration increases the specific heat to a minor extent. The $C_p$ data for the pure crystals (Fig. 12) are good to $\pm$ 1%. Our value of $C_p$ for TGS at 300°K is within the range of values reported in the literature (Ref. 17).

Figures 13-16 summarize the specific heat data for the doped
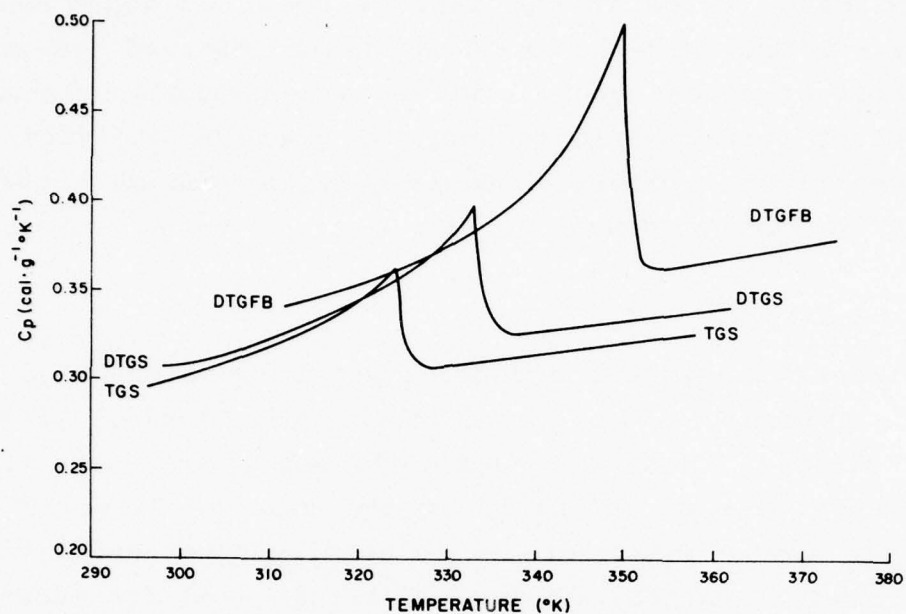
Figure 12. $C_p$ data for pure TGS, DTGS, TGF band DTGFB.
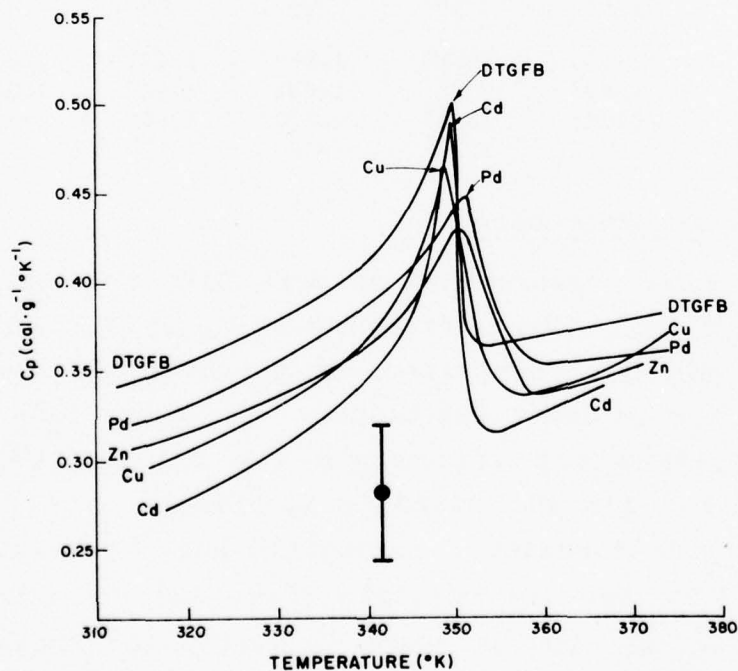


Figure 13. Effect of impurities on $C_p$ of DTGFB (85% D).
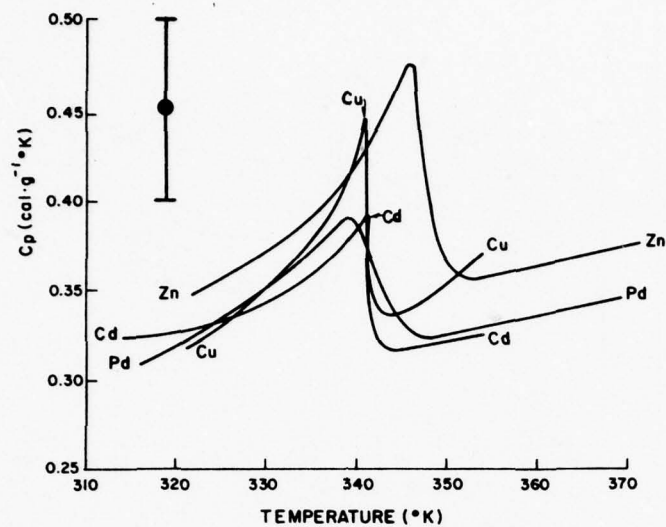
Figure 14. Effects of impurities on $C_p$ of TGFB.
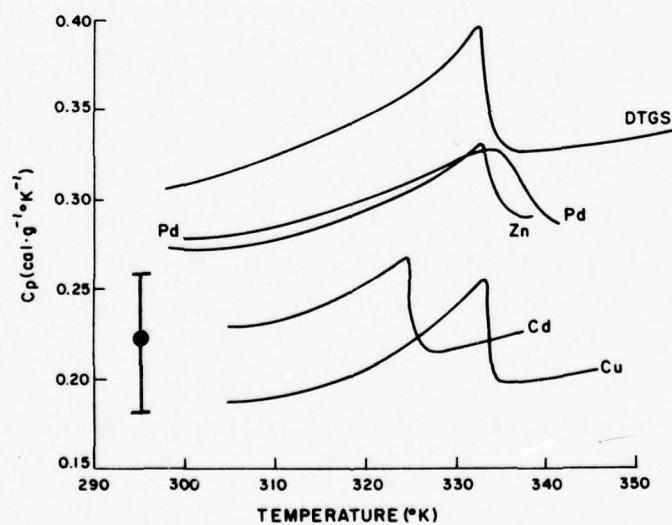


Figure 15. Effects of impurities on $C_p$ of DTGS (90% D).

39
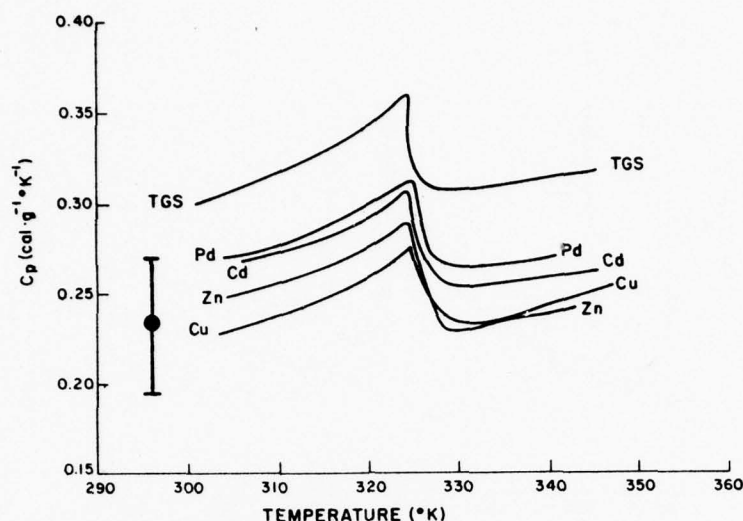
Figure 16. Effects of impurities on $C_p$ of TGS.

crystals. The largest decreases in specific heat are obtained (within a specific family) for Cd doping of DTGFB; and in the case of TGS and DTGS by Cu. The ferroelectric Curie temperatures, determined from the peak of the $C_p$ curve, show that the largest shifts are found in the Pd doped samples which is also accompanied by a pronounced broadening of the curves.

The reduction of $C_p$ for the doped sample, which in some cases amounts to 25%, is probably caused by the dopants but, based on the relatively low concentrations of dopants actually incorporated into these crystals (see Table 8) secondary effects may also play a role.

In general, the effective behavior of the dopants can be classified according to Cd>Cu>Zn>Pd.

A re-measurement of another sample of Cu:DTGS showed an increase in $C_p$. The behavior of $C_p$ as a function of temperature for this new sample approximated the curve for Zn:DTGS. The differences between the doped crystals and pure DTGS, while being in the

order of 10-25% are still within the scatter obtained for different samples taken from the same crystal. The scatter of $C_p$ within a single doped sample was on the order of $\pm$ 15%. This effect could be attributed to dopant inhomogeneity and different concentrations of bulk defects. The effect could not be eliminated due to the small sample size used in the $C_p$ measurement (~10-30 mg).

## 3.4    Thermal Conductivity

The calibration of the thermal conductivity apparatus was checked against a standard sample of Corning Pyrex Type 7740. The measured value was within 2% of that cited for the standard. Considering all potential sources of error for this measurement technique, the thermal conductivity (K) values given in this report are accurate to 5%.

Precision thermal conductivity measurements are difficult to perform and as seen in the literature, values for the same material vary by as much as 50%. Table 10 lists typical reported values of K for TGS measured along the [010]. The close agreement of the values of references 16 and 17 with the present study may be attributed to the fact that the same comparative measurement technique was employed.

TABLE 10.   THERMAL CONDUCTIVITY OF TGS.

$(K \times 10^{-3} cal.s^{-1}.cm^{-1}\,^{\circ}C^{-1})$ [010]

| Temperature °C | K | Reference |
|---|---|---|
| 30 | 1.764 | (15) |
|  | 1.314 | (16) |
|  | 1.568 | (1) |
|  | 1.36 | (17) |
|  | 1.24 $\pm$ 0.06 | Present study. |
| 40 | 1.746 | (15) |
|  | 1.336 | (16) |
|  | 1.587 | (1) |
|  | 1.23 $\pm$ 0.06 | Present study. |
| 50 | 1.744 | (15) |
|  | 1.338 | (16) |
|  | 1.22 $\pm$ 0.06 | Present study. |

41

The variation of thermal conductivity with temperature for TGS and DTGFB in the [010], is illustrated in Figure 17. Over the temperature range of interest for PEV applications, K is found to be essentially independent of temperature. Table 11 compares K for TGS, TGFB and DTGFB. It is clear that DTGFB has the lower thermal conductivity.
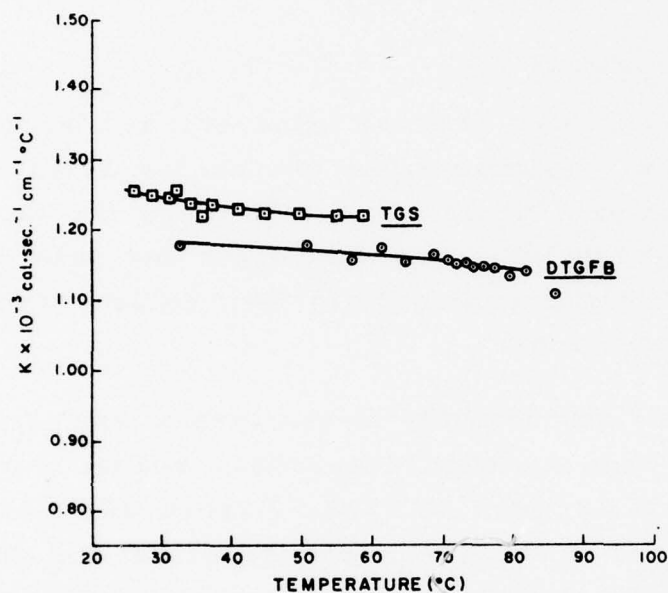


Figure 17. Thermal conductivity of TGS and DTGFB, [010].

TABLE 11. COMPARISON OF THERMAL CONDUCTIVITY FOR PURE TGS, TGFB AND DTGFB.

[010]   $Kx10^{-3}cal.s^{-1}cm^{-1}\circ C^{-1}$ ($\pm$ 5%)

| Temperature °C | (Q&S)<br>TGS | (Isomet)<br>TGFB | (2-188)<br>DTGFB |
|---|---|---|---|
| 30 | 1.24 | 1.29 | 1.18 |
| 35 | 1.24 | 1.28 | 1.17 |
| 40 | 1.23 | 1.28 | 1.17 |
| 45 | 1.22 | 1.26 | 1.16 |
| 48 | 1.23 | 1.29 | 1.17 |
| 53 | 1.22 | 1.29 | 1.16 |
| 56 | 1.22 | 1.28 | 1.16 |

There is another problem with comparing thermal conductivity data from various sources on the same material – how were the crystals grown; purity, etc. Table 12 lists our measured K values for three orientations in a pure TGS crystal obtained from the Isomet Corporation. The values of K in the [010] are

TABLE 12.  THERMAL CONDUCTIVITY
OF TGS PURE (ISOMET).

$Kx10^{-3}cal.s^{-1}cm^{-1}{}^{\circ}C^{-1}$ ($\pm$ 5%)

| Temperature °C | [100] | [010] | [001] |
|---|---|---|---|
| 32 | 1.28 | 1.33 | 1.23 |
| 37 | 1.30 | 1.35 | 1.24 |
| 41 | 1.30 | 1.34 | 1.24 |
| 49 | 1.31 | -- | 1.25 |

8% lower than for a TGS obtained from Quartz & Silice. In addition, the variations of K with crystallographic orientations are smaller than those reported by other investigators (Refs. 1,15,16,17). It is clear that the K data obtained during this program should only be compared with the literature with caution. However, because our crystals were all grown under controlled conditions, fabricated and measured under identical conditions, comparisons of our data are assumed to be relevent.

The thermal conductivity data for the doped crystals grown during this program were measured in only the [010] and at 35°C. This was justified on the basis of the small variation in K with orientation and the temperature independence of K.  Table 13 lists a complete set of data for TGS:Cd.  The difference in K between the [010] and [001] is only about 8% (Table 13) and is temperature independent.  The difference between the [001] and [100], which is important for PEV operations, appears to be on the order of 25%.  Previous data obtained at Philips Labs, during PEV tube operation, did not show a variation for the [001] and [100] orientations.  However, it is doubtful that 25% variations can be observed during tube operation (Ref. 18).

TABLE 13.  THERMAL CONDUCTIVITY OF TGS:Cd.

$(K \times 10^{-3} \text{cal.s}^{-1}\text{cm}^{-1}{}^{\circ}\text{C}^{-1}) \pm 5\%$

| Temperature °C | [010] | [001] | [100] |
|---|---|---|---|
| 36 | 1.12 | 1.02 | 1.32 |
| 42 | 1.13 | 1.05 | 1.30 |
| 49 | 1.12 | 1.02 | 1.38 |
| 55 | 1.14 | 1.06 | 1.34 |
| 65 | 1.12 | 1.03 | 1.35 |

The thermal conductivity of all doped crystals are summarized in
Table 14.

TABLE 14.  DOPED TGS TYPE CRYSTALS.  SUMMARY OF
THERMAL CONDUCTIVITY MEASUREMENTS [010] 35°C.

$(K \times 10^{-3}\text{cal.s}^{-1}\text{cm}^{-1}{}^{\circ}\text{C}^{-1} \ (\pm 5\%))$

| Crystal | K | Crystal | K |
|---|---|---|---|
| TGS | 1.24 | TGFB | 1.28 |
| TGS:Cu | 1.23 | TGFB:Cu | 1.23 |
| TCS:Zn | -- | TGFB:Zn | 1.17 |
| TGS:Pd | -- | TGFB:Pd | 1.20 |
| TGS:Cd | 1.12 | TGFB:Cd | 1.29 |
| | | | |
| DTGS | 1.30 | DTGFB | 1.18 |
| DTGS:Cu* | 1.24 | DTGFB:Cu | 1.12 |
| DTGS:Zn | 1.08 | DTGFB:Zn | 1.10 |
| DTGS:Pd | -- | DTGFB:Pd | 1.36 |
| DTGS:Cd* | 1.35 | DTGFB:Cd | 1.13 |

*small cracks parallel [010]

The lowest values within one family, were obtained for TGS:Cd;
DTGS:Zn; TGFB:Zn and DTGFB:Zn.  It would appear that even at the
low Zn levels in these crystals that significant reduction in K
can be achieved.  Higher doping levels of Zn would prove inter-
esting and should be investigated.

## 3.5    Thermal Diffusivity

The calculated values for thermal diffusivity (k) of the doped
crystals are summarized in Table 15.   The k values were calcu-
lated from Equation (3).   It is clear that the Zn dopings of

TABLE 15.   COMPARISON OF THERMAL DIFFUSIVITY
(k) FOR DOPED TGS TYPE CRYSTALS ([010], 35°C).

| Crystal | $k \times 10^{-3} cm^2/s$ | | Crystal | $k \times 10^{-3} cm^2/s$ | |
|---|---|---|---|---|---|
| TGS | 2.3 | +10% | DTGS | 2.3 | +10% |
| TGS:Cd | 2.4 | } +20% | DTGS:Cu | 3.7 | |
| TGS:Cu | 3.0 | | DTGS:Zn | 2.2 | +20% |
| | | | DTGS:Cd | 3.5 | |
| | | | | | |
| TGFB: | 2.1 | +10% | DTGFB | 1.8 | +10% |
| TGFB:Cu | 2.0 | | DTGFB:Cu | 1.9 | |
| TGFB:Zn | 1.8 | +20% | DTGFB:Zn | 1.9 | +20% |
| TGFB:Cd | 2.2 | | DTGFB:Cd | 2.1 | |
| TGFB:Pd | 2.0 | | DTGFB:Pd | 2.2 | |

TGFB and DTGS has the greatest effect.   The measurement of k, in
a PEV tube, for pure DTGFB range from $1.7 \times 10^{-3}$ to $3.0 \times 10^{-3}$ and is probably influenced by deuteration (Ref. 18).
This variation is observed for DTGFB crystals obtained from
different sources.   The values of k from tubes measured at
Philips Laboratories for pure TGS and TGFB are $2.8 \times 10^{-3}$ and
$2.0 \times 10^{-3}$, respectively (Ref. 18).

Table 16 lists the thermal diffusivity (k) for pure TGS obtained
from various sources and compares TGS:Cd against these values.
The evaluation of this data should be restricted to the differ-
ences in k between the [100] and [001] orientations, which lie
in the plane of PEV target.   From the table, we see that  k
varies in magnitude from 5 to 36% and that for one sample the
value of k increased (+36%).   The reason for the large varia-
tions observed in k can probably be attributed to crystal
quality (i.e., perfection) and crystal growth history.   Our k
data for TGS:Cu was compared with that reported by Krajewski, et
al (Ref. 19).   Table 17 lists their k values for pure and
metal doped TGS.   Our k value of 3.0, for Cu:TGS (35 ppm),

## TABLE 16.  THERMAL DIFFUSIVITY* OF TGS AND TGS:Cd.

$$*(k \times 10^{-3} cm^{-2}/s)$$

| Orientation | TGS:Cd | Philips | Isomet | Helwig & Albers[16] | Coronel & Gonzalo[17] | Kajewski & Jaroszyk[2] | Krajewski & Riad[3] |
|---|---|---|---|---|---|---|---|
| $k_{100}$ | 2.86 | 2.41 | 2.41 | 2.77 | 2.49 | 2.41 | 4.05 |
| $k_{010}$ | 2.39 | 2.49 | 2.30 | 2.43 | 2.52 | 2.91 | 3.50 |
| $k_{001}$ | 2.22 | 2.28 | 1.97 | 2.23 | 3.38 | 1.65 | 3.20 |
| **Δk** | | | | | | | |
| [100]->[001] | -22% | -5% | -18% | -19% | +36% | -31% | -21% |
| [010]->[001] | - 7% | -8% | -14% | - 9% | -34% | -44% | +16% |
| [010]->[100] | +20% | -3% | + 5% | +14% | -0.7% | -17% | - 9% |

## TABLE 17.  THERMAL DIFFUSIVITY OF PURE AND DOPED TGS[19].

| Sample | [100] | [010] | [001] |
|---|---|---|---|
| | ---------- | (k×10^{-3}cm^{-2}/s) | -------- |
| TGS (pure) | 3.90 | 3.56 | 3.14 |
| TGS:Cu 10 ppm | 3.46 | 3.25 | 2.73 |
| TGS:Cu 80 ppm | 2.98 | 2.88 | 2.46 |
| TGS:Cu 270 ppm | 2.47 | 2.38 | 2.10 |
| TGS:Cr 4 ppm | 3.47 | 3.28 | 2.85 |

agrees well with their values for Cu dopings in the same concentration range.  It should be noted that they observe an overall decrease in k, for all orientations, of >30%.  The effect is definitely dependent on metal ion concentration.

Recent data from Krajewski on organic doping of TGS are given in Table 18 only for information.  It is clear that their work is now shifting to include organic modifiers.  Another reason for

TABLE 18. THERMAL DIFFUSIVITY OF ORGANIC DOPED TGS[20].

| Sample | ---------- $(kx10^{-3}cm^{-2}/s)$ -------- | | |
| | [100] | [010] | [001] |
| TGS (pure) | 3.90 | 3.56 | 3.14 |
| TGS:L(+)Alanine 200 ppm | 3.60 | 2.88 | 2.77 |
| TGS:p-nitroaniline 18 ppm | 3.98 | 3.62 | 3.24 |
| TGS:o-nitroaniline 26 ppm | 3.88 | 3.60 | 3.31 |
| TGS:m-nitroaniline 40 ppm | 3.78 | 3.45 | 3.17 |

this direction is evident from a recent publication of Eisner (Ref. 21). He claims that aniline doping of TGS significantly increases the pyroelectric effect in TGS by about a factor of 2.5.

In summary, the scatter of results for thermal diffusivity are disturbing, however, the evidence is clear that metal dopings do effect this property - even at the low concentrations obtained in this present study! Further investigations at higher doping levels of both metallic and organic compounds are warrented.

3.6    Accuracy of Experimental Electrical Data

The pyroelectric coefficient is determined by measuring current and temperature as a function of time. The current, $I_p$, is divided by the electrode area and the graphically measured time derivative of temperature. A worst case analysis of all of the measurement steps predicts an absolute accuracy of $\pm$ 25% for p. In practice we have measured reproducibilites of $\pm$ 5% for the same sample and $\pm$ 10% from sample-to-sample for the same material.

A similar analysis for the dielectric constant gives accuracy limits of $\pm$ 15% with a precision of 5%. Reproducibilities of better than 3% are routine.

Temperature is measured to a precision of 0.3°C with an accuracy of 0.5°C. However, since our data are necessarily collected on heating or cooling an addition temperature correction of $\pm$ 1°C is possible due to lag errors.

Because both p and $\varepsilon$ are rapidly changing in the vicinity of the phase transition (7° in Fig. 18), lag errors can produce anamolies in the p/$\varepsilon$ ratio that could be nothing more than artifacts. Precise determination of these effects is possible but outside the scope of the present investigation.

Ferroelectric hysteresis loops determined by oscilloscope traces are limited to a reading accuracy of $\pm$ 5% and an overall accuracy of $\pm$ 25%. Reproducibilities to better than $\pm$ 10% are routine.

### 3.7    Pyroelectric Data

The pyroelectric coefficients for the TGS, DTGS, TGFB and DTGFB families of crystals are shown in Figures 18 to 21, respectively. The observed variations in p within a family of doped crystals is less than $\pm$ 5% for DTGS and less than $\pm$ 10% for TGS, TGFB and DTGFB.

The data were collected on cooling; rates were within the range of 0.5°C/min to 1.5°C/min. As expected, the pyroelectric coefficient was not dependent on the temperature rate of change.

Figure 18. Pyroelectric coefficient as a function of temperature for TGS type crystals.

49

Figure 19. Pyroelectric coefficient as a function of temperature for DTGS type crystals.
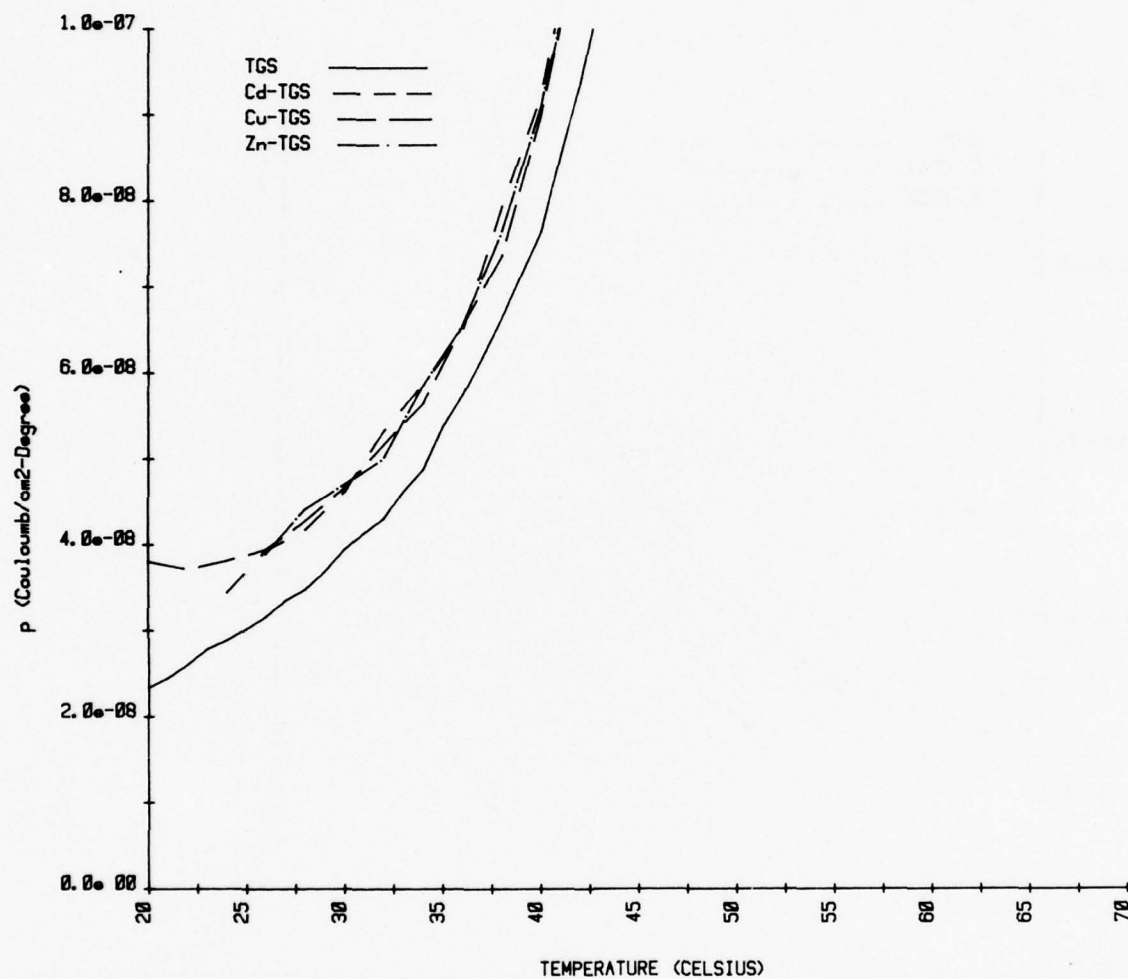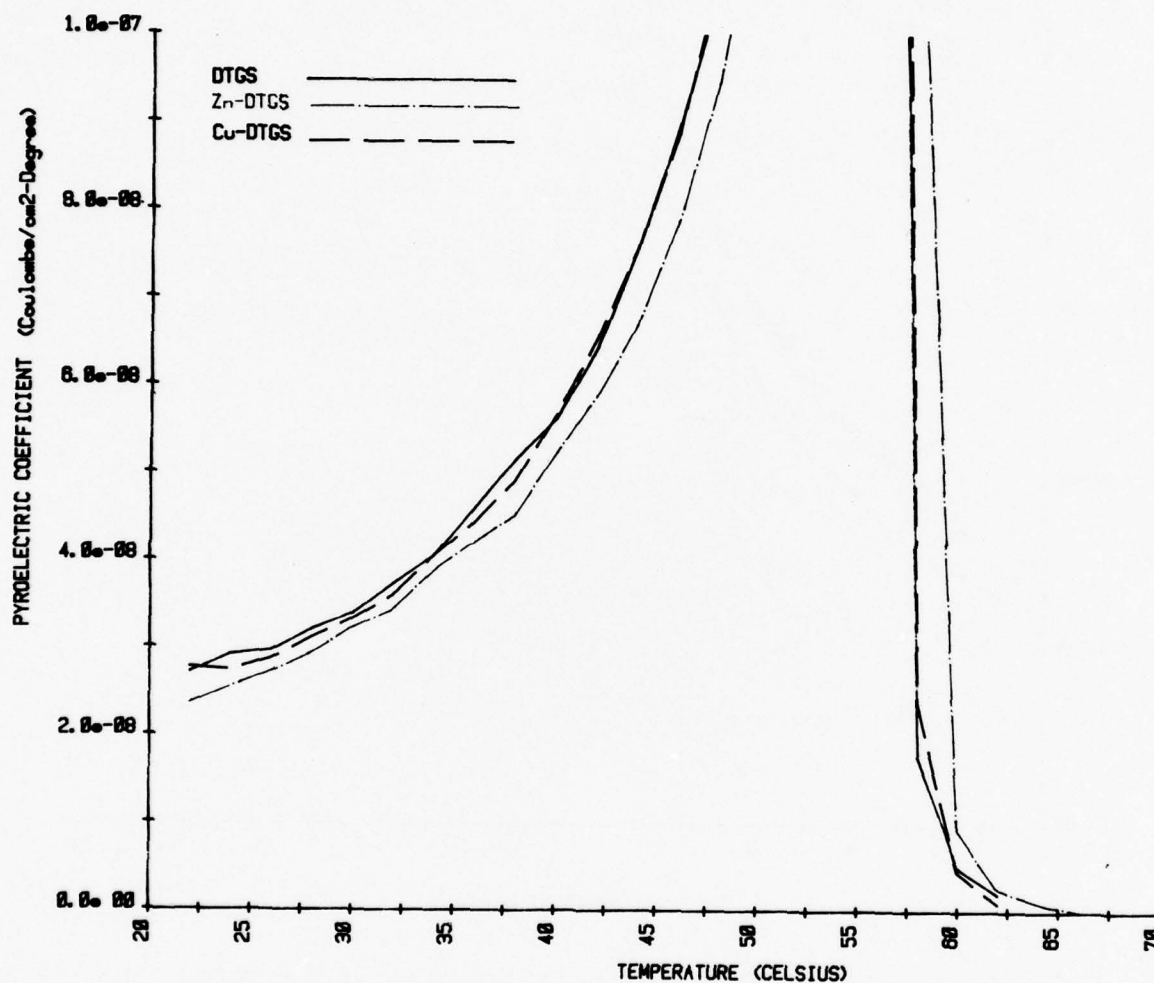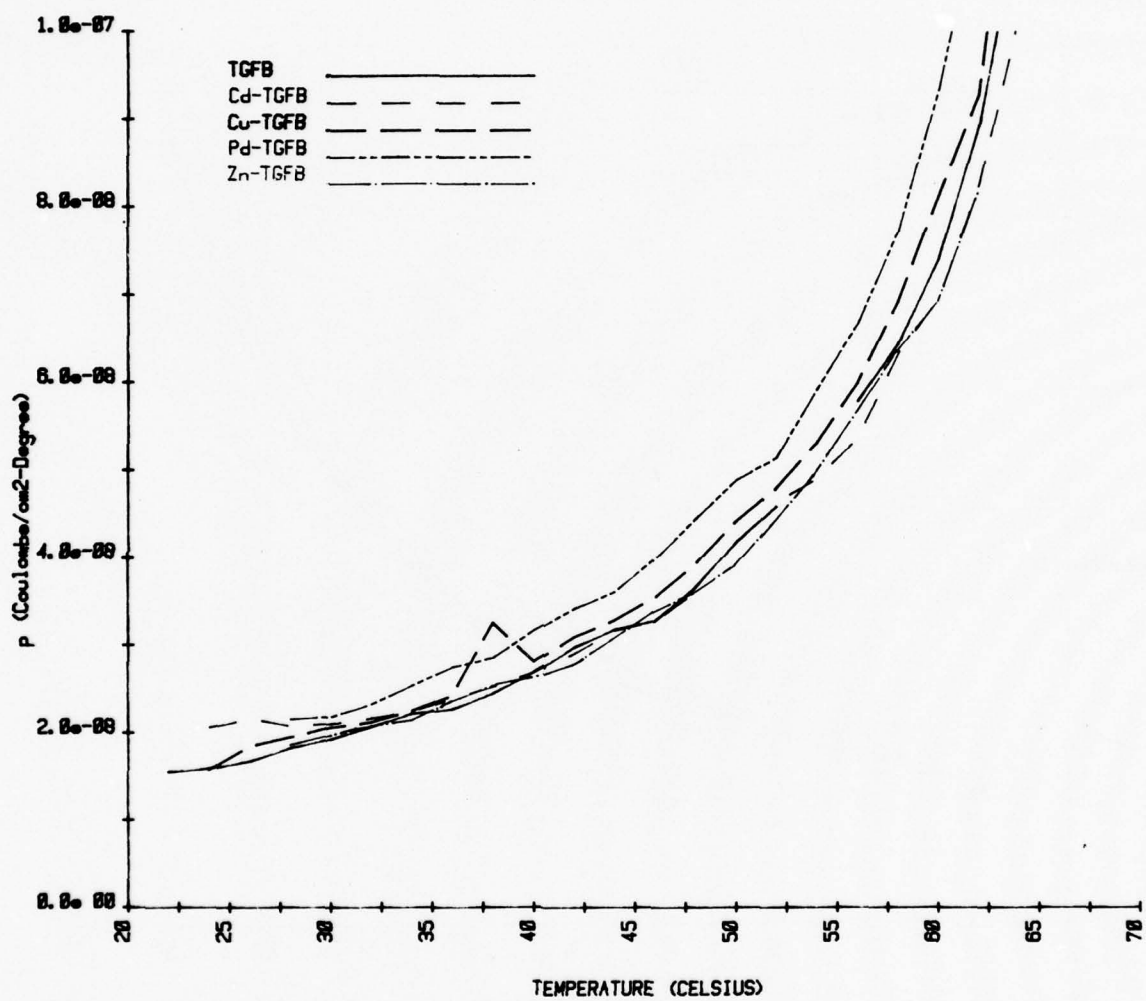
Figure 20. Pyroelectric coefficient as a function
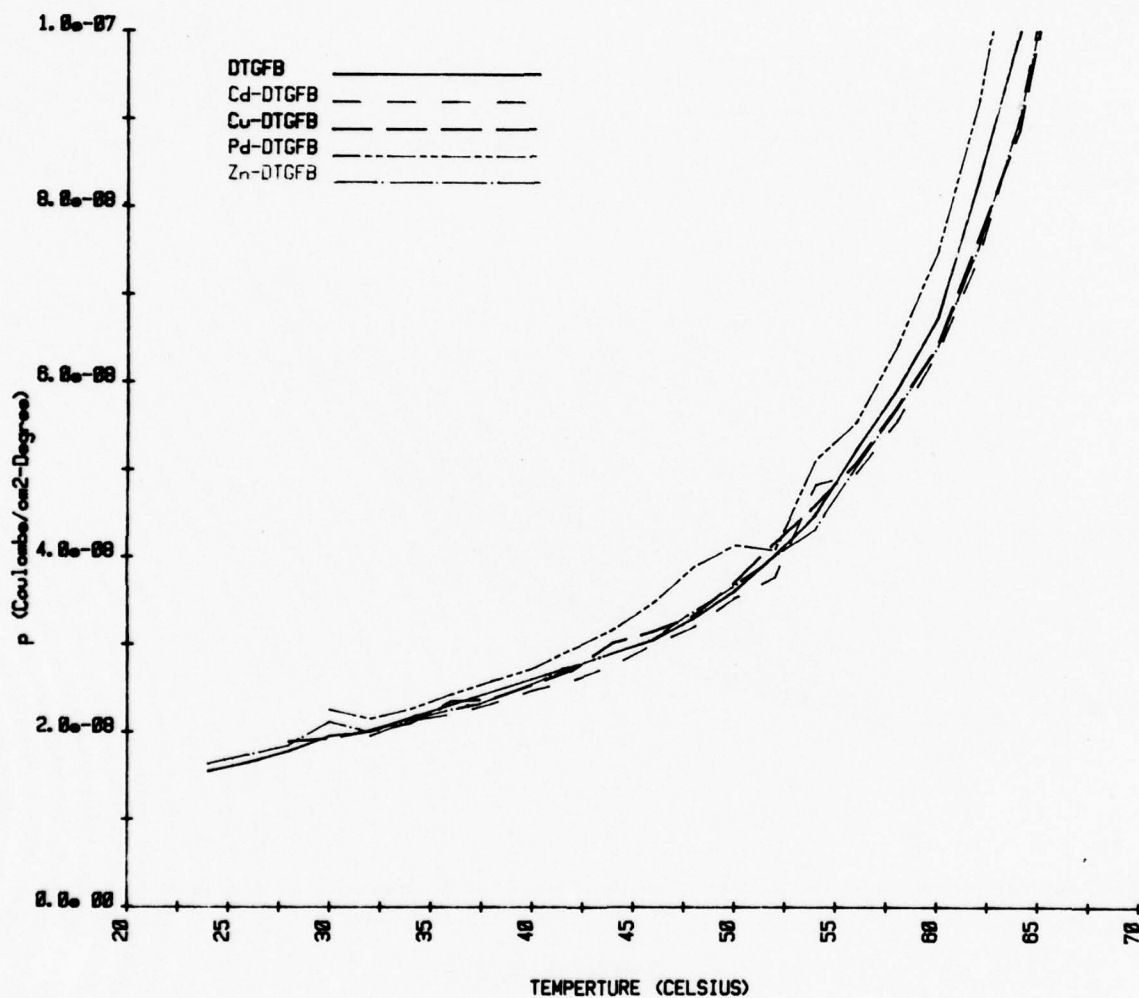of temperature for TGFB type crystals.

Figure 21.   Pyroelectric coefficient as a function
of temperature for DTGFB type crystals.

## 3.8    Dielectric Constants

Dielectric constants as a function of temperature are given in Figures 22 to 25 for the TGS, DTGS, TGFB and DTGFB families, respectively.  For temperatures removed from the vicinity of $T_c$ the observed variations of dielectric constant within a family of crystals is less than $\pm$ 10%.

The Curie temperatures as characterized by the peak dielectric constants are given in Table 19.  No systematic effect of doping on $T_c$ is observed.

TABLE 19.  SUMMARY OF CURIE TEMPERATURES
OF TGS TYPE CRYSTALS.

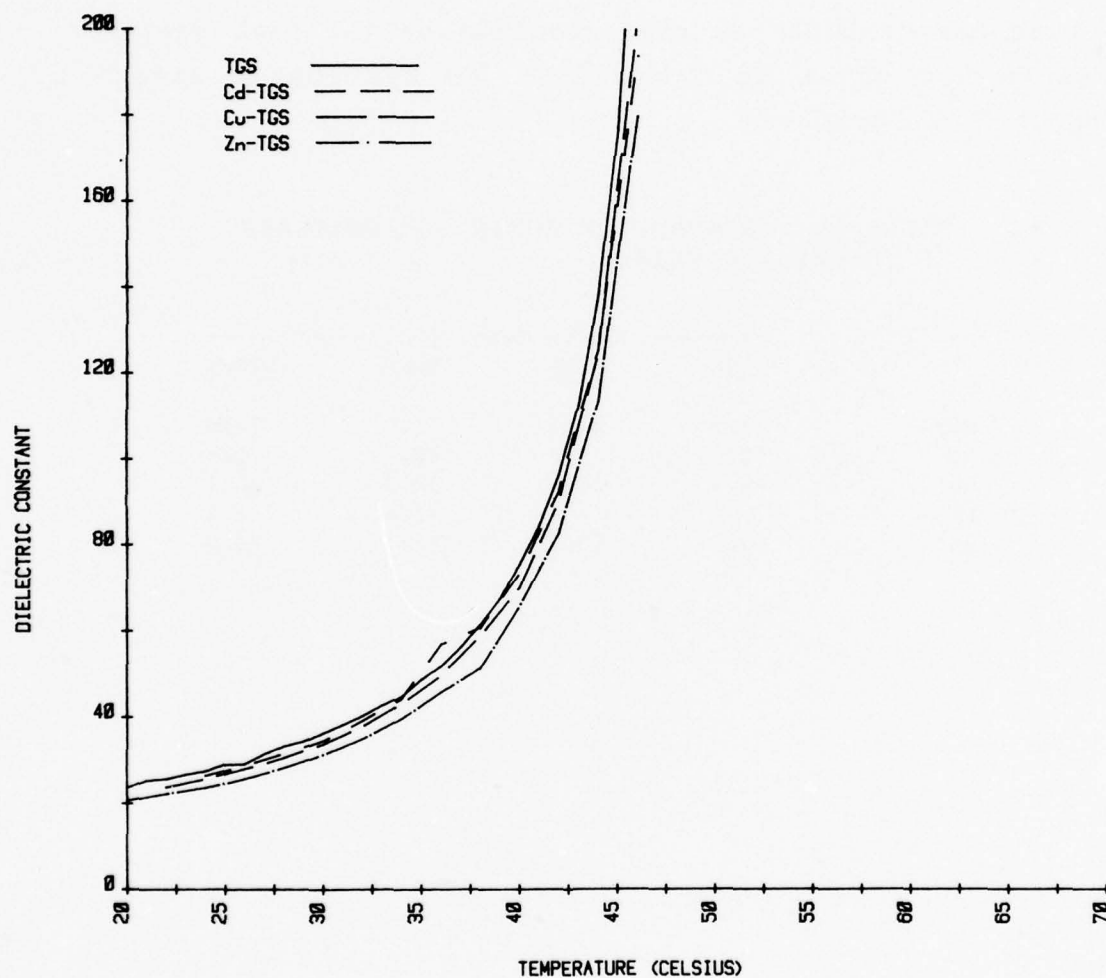| | ----------Curie Temp. (°C)----------- | | | |
| | TGS | DTGS | TGFB | DTGFB |
|---|---|---|---|---|
| Pure | 49.9 | 57.3 | 73.0 | 73.6 |
| Cd | 50.0 | -- | 74.2 | 74.0 |
| Cu | 49.5 | 57.6 | 72.3 | 75.1 |
| Pd | -- | -- | 71.6 | 74.2 |
| Zn | 50.0 | 58.5 | 72.7 | 74.2 |

53

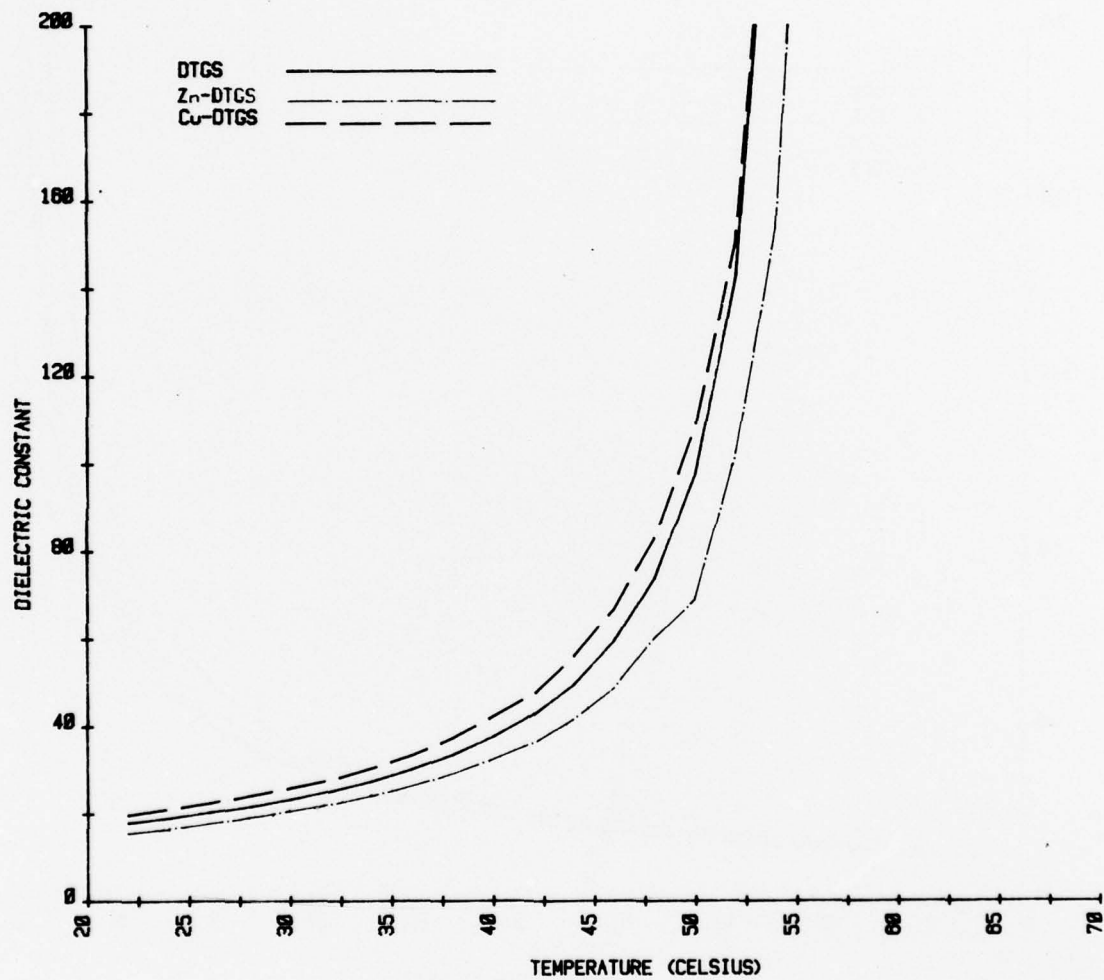Figure 22.  Dielectric constant vs. temperature for
TGS family crystals.

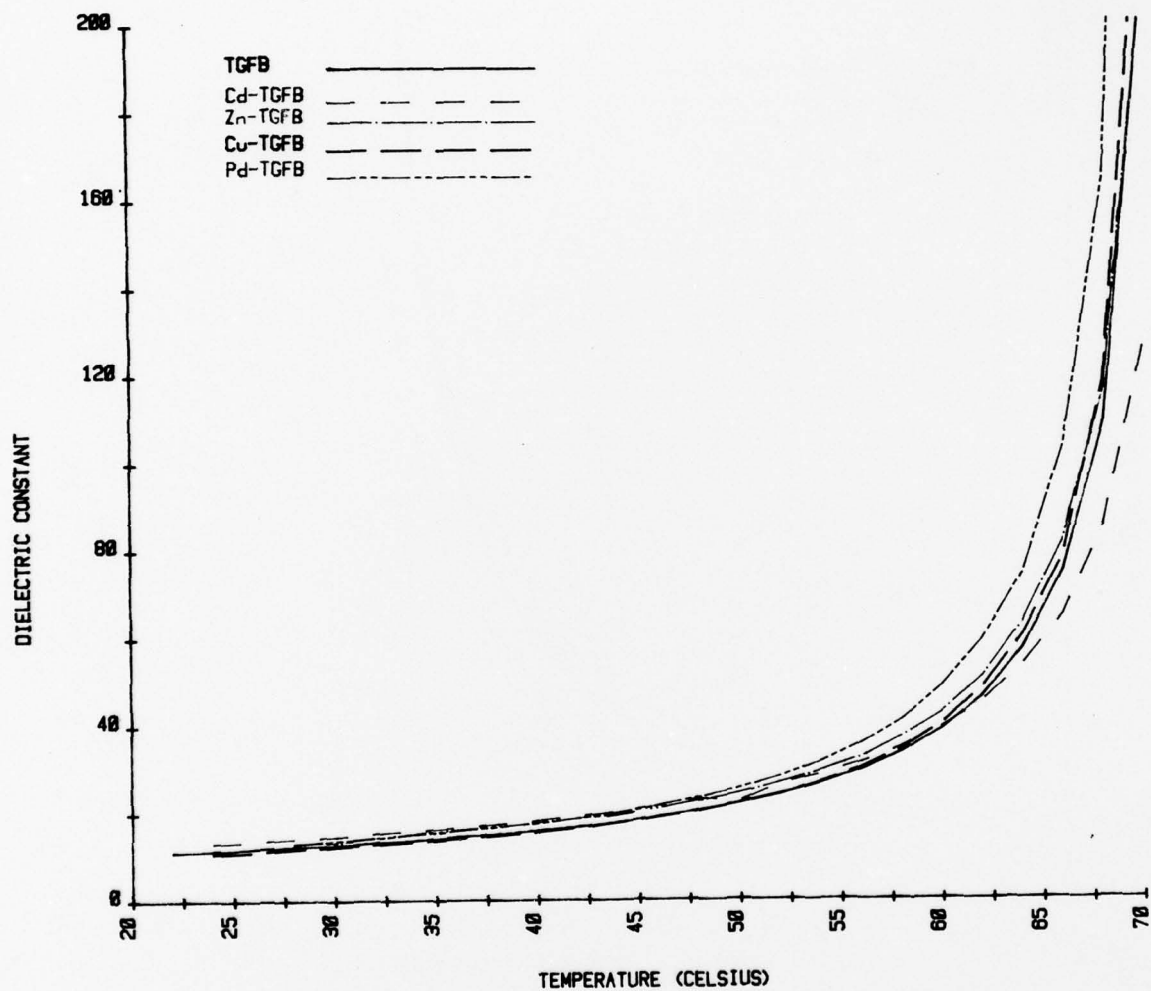Figure 23.   Dielectric constant vs. temperature for
DTGS family crystals.

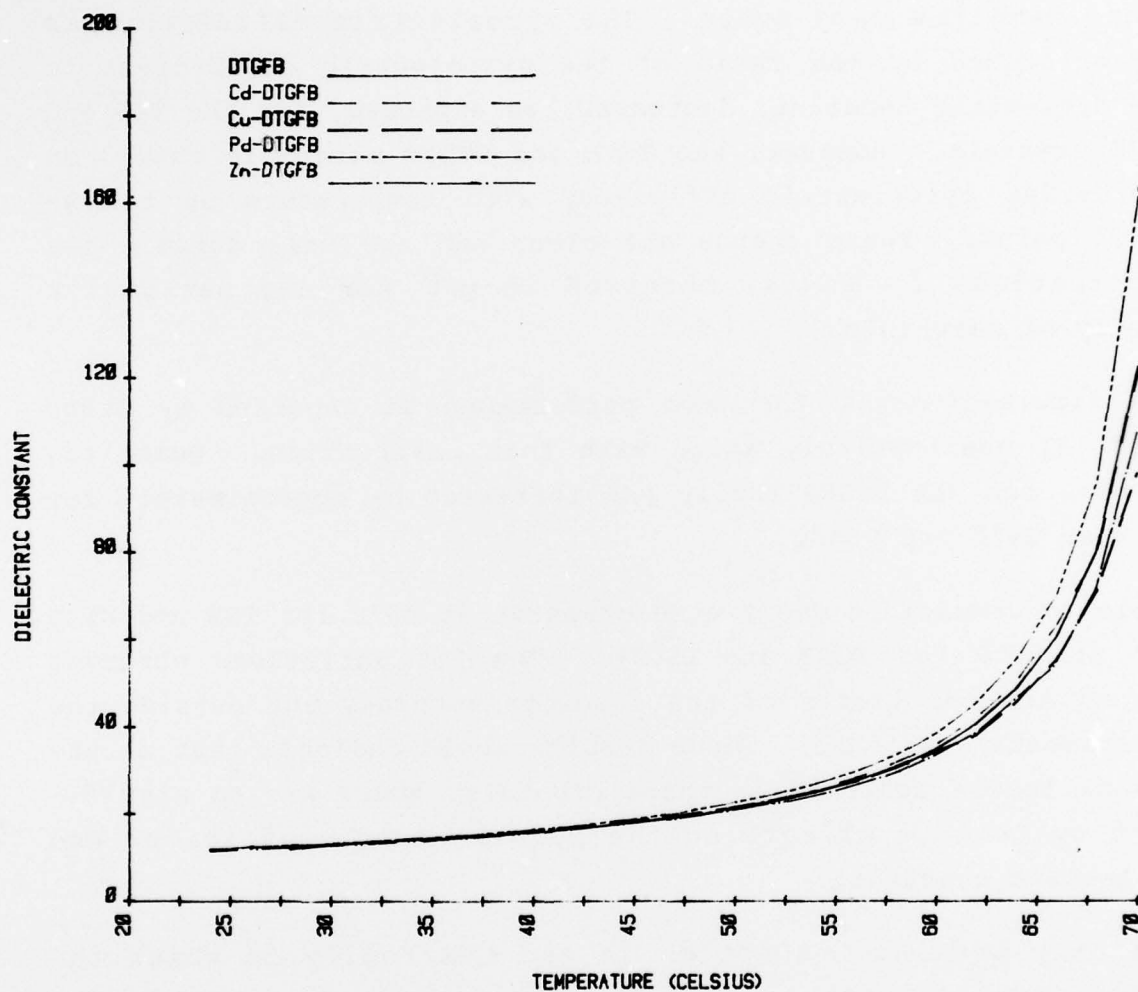Figure 24. Dielectric constant vs. temperature for TGFB family crystals.

Figure 25. Dielectric constant vs. temperature for DTGFB family crystals.

## 3.9 Pyroelectric Efficiency

The pyroelectric efficiencies ($p/\varepsilon$) for doped TGS, DTGS, TGFB and DTGFB crystals are given in Figures 26 to 29, respectively.

For the doping levels obtained in the measured crystals pyroelectric efficiency showed few changes. However, a few significant anamolies were noted. The pyroelectric efficiency, as characterized by the ratio of the pyroelectric coefficient to the dielectric constant, decreased, as expected, for the TGS and DTGS crystals. However, the TGFB and DTGFB materials showed an increasing pyroelectric efficiency with temperature up to the Curie point. These trends are clear and are well outside the fluctuations ($\sim \pm 10\%$) observed in $p/\varepsilon$ for any particular family of materials.

The figure-of-merit for tube performance as reported by Stupp (Ref. 5) qualitatively agree with this observation. Quantitatively, for the DTGFB family $p/\varepsilon$ increases by approximately 25% between 25°C and 65°C.

Table 20 summarizes the figure-of-merit at 40°C for TGS and DTGS and at 60°C for TGFB and DTGFB. The 25% variations observed are within the limits of the absolute accuracy but outside the experimental varience. These results would indicate that at the doping levels achieved in these crystals, there are no significant systematic effects on the pyroelectric coefficient and dielectric constant.

The only possible exception is the TGS family in which the pyroelectric coefficient of the doped crystals is typically higher than samples of pure TGS (Fig. 18). However, since the data of Figure 18 only represent five samples, the differences between doped and undoped samples has very little statistical significance and should be considered as suggestive.

## TABLE 20. SUMMARY OF FIGURE-OF-MERITS OF TGS TYPE CRYSTALS.

$p/\varepsilon$ C/cm$^2$-degree x 10$^{-9}$

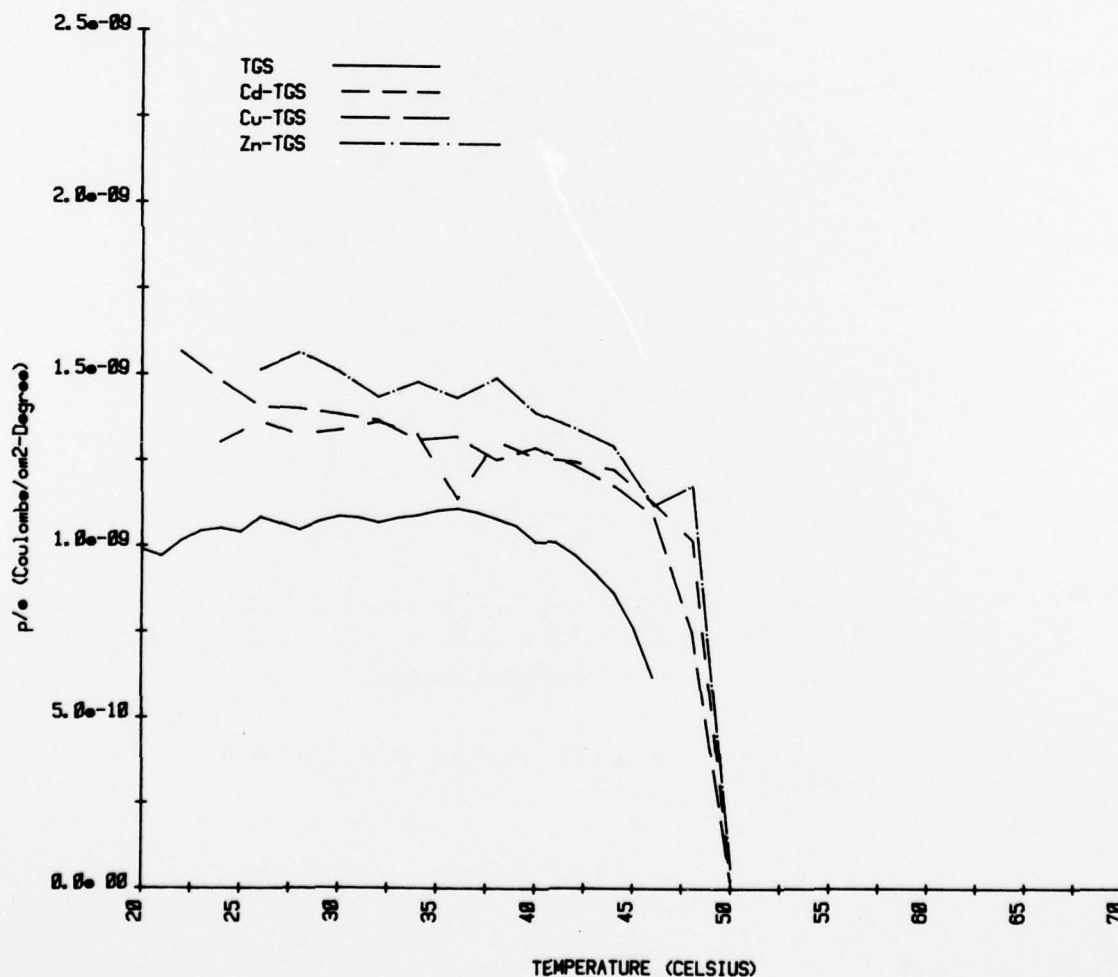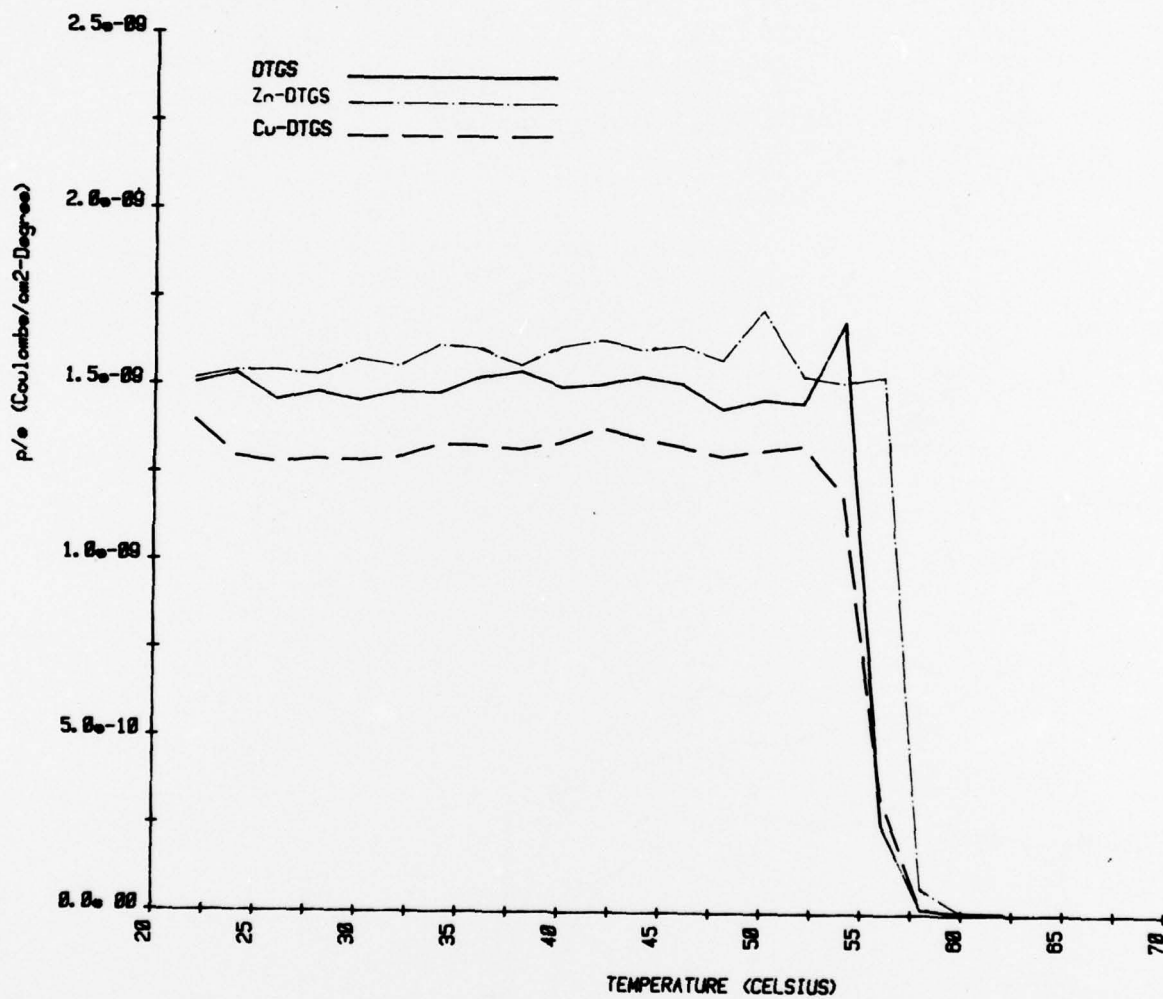| | ----at 40°C---- | | ----at 60°C----- | |
|---|---|---|---|---|
| | TGS | DTGS | TGFB | DTGFB |
| Pure | 1.00 ±.1 | 1.50 +.14 | 1.90 +.14 | 1.94 +.14 |
| Cd | 1.28 +.14 | -- | 1.72 | 1.75 |
| Cu | 1.28 +.14 | 1.36 | 1.98 | 1.87 |
| Pd | -- | -- | 1.90 | 1.94 |
| Zn | 1.41 +.14 | 1.61 | 1.71 | 1.94 |



Figure 26. Pyroelectric efficiency p/ε for TGS family materials.
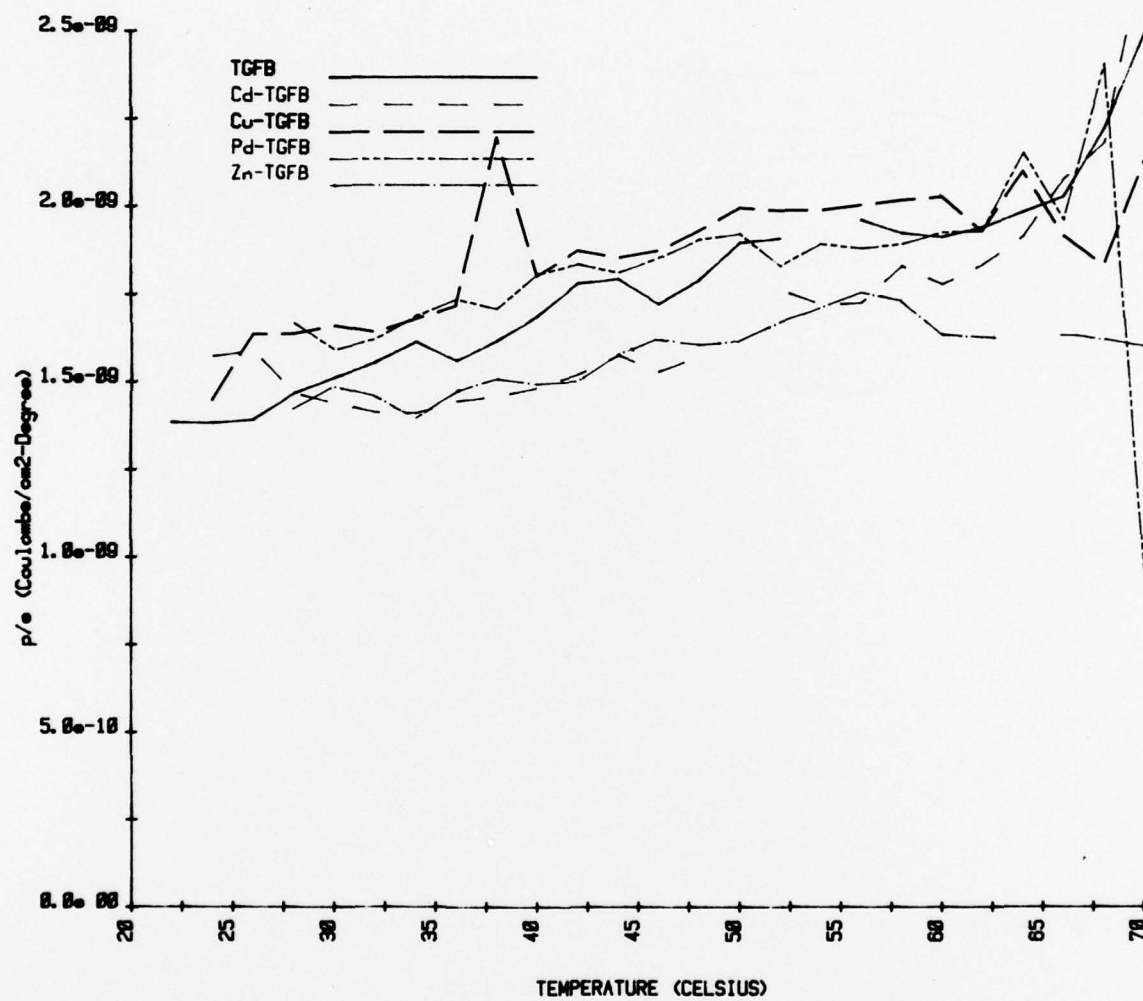
Figure 27. Pyroelectric efficiency p/ε for DTGS
family materials.

Figure 28. Pyroelectric efficiency p/ε for TGFB family materials.
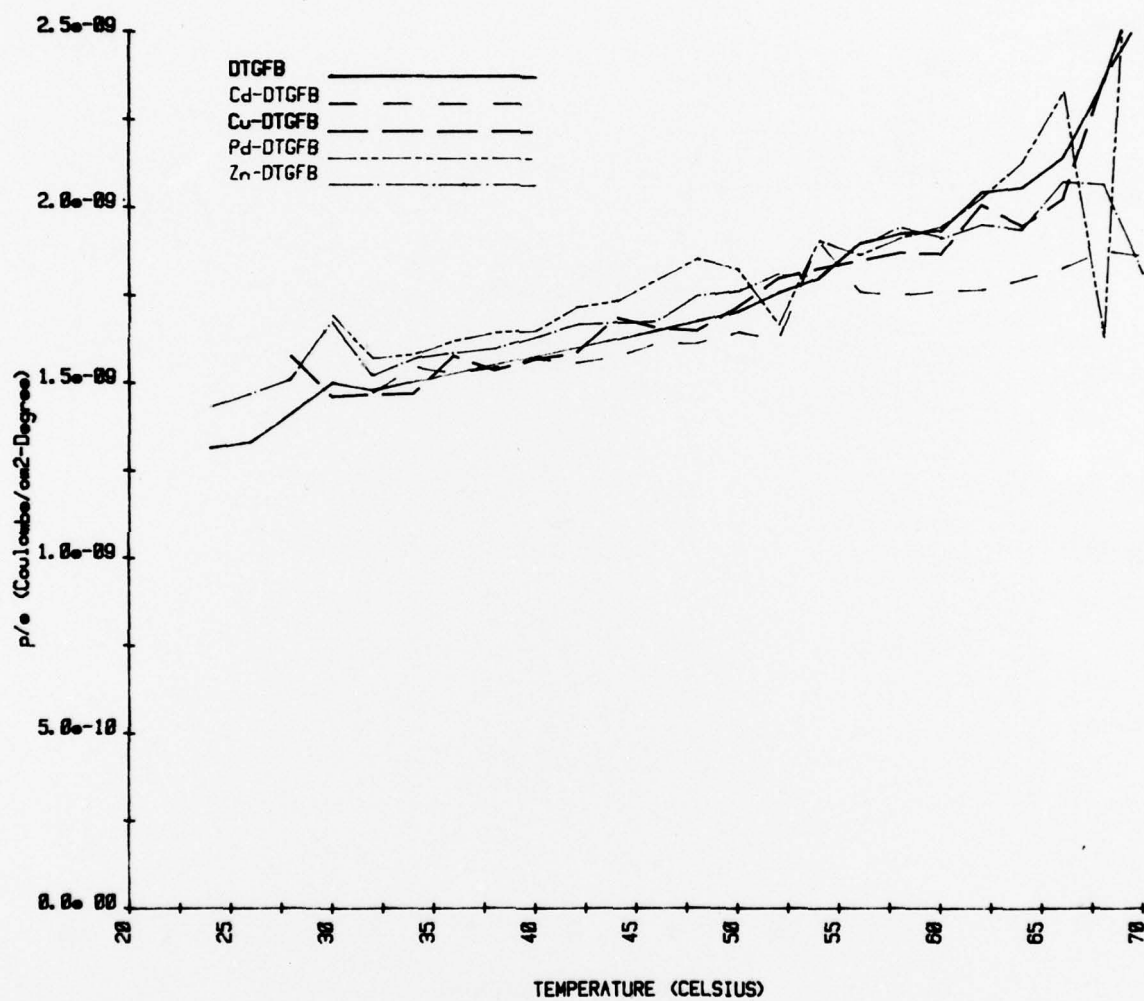
Figure 29.  Pyroelectric efficiency p/ε for DTGFB
family materials.

62

## 3.10     Spontaneous Polarization

The spontaneous polarization ($P_s$) of the doped and pure crystals was determined from ferroelectric hysteresis loops and from integration of the pyroelectric current. A typical hysteresis loop is shown in Figure 30. Table 21 gives $P_s$ for the crystals studied. Agreement between the two techniques agreed to usually better than $\pm$ 10%.

This agreement verifies that $I_p$ was being measured for a poled sample. The observed fluctuations in $P_s$ are within the expected accuracy. No systematic effects of doping on $P_s$ are seen.

TABLE 21. COMPARISON OF SPONTANEOUS POLARIZATION ($\mu$coul/cm$^2$) AT 24°C AS MEASURED BY TWO METHODS, HYSTERESIS LOOPS/INTEGRATION OF PYROELECTRIC CURRENT.

|      | TGS | DTGS | TGFB | DTGFB |
|------|------|------|------|-------|
| Pure | 2.9/3.0$\pm$.25 | 3.1/3.2$\pm$.3 | 4.0/4.1$\pm$.4 | 4.0/4.1$\pm$.4 |
| Cd   | 2.5/2.7 | --- | 3.7/3.6 | 4.0/4.0 |
| Cu   | 2.3/2.6 | 3.2/3.2 | 4.1/4.3 | 4.4/4.3 |
| Pd   | --- | --- | 3.7/4.1 | 4.7/4.5 |
| Zn   | 2.8/2.8 | 3.3/3.2 | 4.1/4.6 | ---/4.5 |



Figure 30. Typical hysteresis loop for TGS.

## 4.    CONCLUSIONS AND RECOMMENDATIONS

The reduction of thermal diffusivity by impurity doping, even in
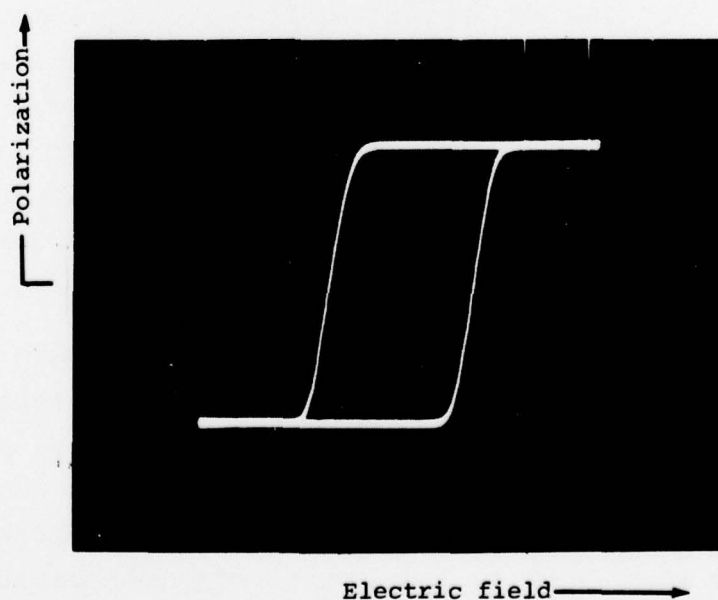the low ppm region, was demonstrated, and these results are
comparable with the literature (Refs. 19,20).  In the case of
the electrical properties of these materials, variations were
typically on the order of 10-15%.  Our measurements were
performed under "tube" boundary conditions (see Par. 2.2.6
and 2.2.7).  Our test conditions, therefore, differ from those
generally reported in the literature (Refs. 4,6).  Sample-to-
sample variations have recently been reported (Ref. 22) for the
measurement of p and $\varepsilon$ in TGS; we have observed similar results
for TGS.  Thus, differences in pyroelectric figure-of-merit of
< 25% must be interpreted with caution.  The same behavior is
also applicable to DTGS, TGFB and DTGFB.  Samples of the doped
crystals were supplied.

The electrical data presented  on TGS and doped-TGS represent
a small statistical sample ($\sim$3 of pure TGS) and, therefore,
have little statistical significance, but the results suggest
possible improvement of the figure-of-merit.  It would be
advisable to grow several of the host materials (i.e., TGS and
DTGFB) from solutions of higher ($\sim$20 mole %) impurity con-
centration and re-measure their thermal and electrical proper-
ties.  Growth from these high dopant level solutions should
result in crystals with dopant levels on the order of several
hundred ppm.  In addition, the large increases in p from the
substitution of organic dopants (Ref. 21) should be investi-
gated.

In view of the large variations (sample-to-sample) in pyro-
electric coefficient, dielectric constant and thermal dif-
fusivity in TGS, as discussed above, a comprehensive program to
establish a true TGS standard is required.  The differences
between the properties obtained in this study and those cited in
the literature can only be qualitatively evaluated.  These
differences may be significant when compared with a reliable
standard.

5.    <u>REFERENCES</u>

1.  T. Krajewski and F. Jaroszyk, Acta. Phys. Pol. <u>A43</u>, 831 (1973).

2.  T. Krajewski and F. Jaroszyk, Acta. Phys. Pol. <u>A43</u>, 845 (1973).

3.  T. Krajewski and M. Riad, Acta. Phys. Pol. <u>A48</u>, 649 (1975).

4.  J. Stankowska, Acta, Phys. Pol. <u>A43</u>, 603 (1973).

5.  E.H. Stupp, Final Technical Report on Contract No. DAAG53-75-C-0256, August (1976).

6.  S. Hayden, G.M. Loiacono, J.F. Balascio and A. Idleson, Proc. Electro-Optical Sys. Design Conf., Nov. 5-7, San Francisco, Calif., 81-86 (1974).

7.  J. Stankowska and M. Krysinska, Acta. Phys. Pol. <u>A40</u>, 239 (1971).

8.  H. Toyoda, Y. Tanaka and W. Shiokawa. Rev. Elec. Comm. Lab. <u>9</u> (7-8), 485 (1961).

9.  J. Moravec, N. Novotny and M. Strajblova, Czech. J. Phys. <u>B23</u>, 855 (1973).

10.  G.M. Loiacono, unpublished data.

11.  S.C. Hayden, J.F. Balascio and G.M. Loiacono, Proc. Electro-Optical Sys. Design Conf., Nov., 5-7, San Francisco, Calif., 26-30 (1974).

12.  M.S. Tsedrick and E.M. Kravchenya, Krist wd. Tech. <u>11</u> (1), 49 (1976).

13.  J. Stankowska, Acta. Phys. Pol. <u>31</u> (3), 527 (1967).

14.  F. Warkusz and K. Lukaszewicz, Bull. Acad. Polon. des. Sci. <u>21</u> (9), 669 (1973).

15.  E.N. Dimarova and Y.M. Poplavko, Sov. Phys., Solid State, <u>6</u>, 2293 (1965).

16.  J. Helwig and J. Albers, Phys. Stat. Sol. <u>A7</u>, 151 (1971).

17.  G. Coronel and J.A. Gonzalo, Ferroelectrics <u>4</u>, 19 (1972).

18.  E.H. Stupp, B. Singer and T. Conklin, IEDM Technical Digest, 559 (1976).

19.  T. Krajewski, F. Jaroszyk and M.A. Riad, Acta. Univ. Wartislaviensis, <u>25</u>, 71 (1977).

20.  T. Krajewski, private communication (1977).

21.  J. Eisner, Phys. Stat. Sol. <u>A43</u>, K1 (1977).

22.  P. Felix, P. Gamot, P. Lacheau, and Y. Raverdy, Ferro-electrics <u>17</u>, 543 (1978).

# DISTRIBUTION LIST

Defense Documentation Center
Attn: DDC-TCA
Cameron Station, Bldg 5
Alexandria, VA 22314
    (12 copies)

Director
National Security Agency
ATTN: TDL
Fort George G Meade, MD 20755

Office of Naval Research
Code 417
Arlington, VA 22217

Director
Naval Research Laboratory
ATTN: Code 2627
Washington, D.C. 20375

Commander
Naval Electronics Laboratory Center
ATTN: Library
San Diego, CA 92152

Commander
US Naval Surface Weapons Laboratory
ATTN: Dr. F. Bis
White Oak, Silver Spring, MD 20910

Commander
Marine Corps
HQ, US Marine Corps
ATTN: Code LMC
Washington, D.C. 20380

Air Force Avionics Laboratory
ATTN: AFAL/TSR, STINFO
Wright-Patterson Air Force Base
Ohio 45433

HQDA (DACE-CMS)
Washington, D.C. 20310

OSASS-RD
Washington, D.C. 20310

CDR, US Army Material Command
ATTN: AMCMA-EE
5001 Eisenhower Avenue
Alexandria, VA 22333

CDR, US Army Material Command
ATTN: AMCRD-FW
5001 Eisenhower Avenue
Alexandria, VA 22333

Commander
US Army Missile Command
ATTN: AMSMI-RR,
       Dr. J. P. Hallowes
Redstone Arsenal, AL 35809

Commander
US Army Armament Command
ATTN: AMSAR-RDP (Library)
Rock Island, IL 61201

Commander
Picatinny Arsenal
ATTN: SARPA-TS-S #59
Dover, N.J. 07801

Commander
Frankford Arsenal
ATTN: Dr. William McNeill PDS
Philadelphia, PA 19137

Commander
USASA Test & Evaluation Center
Fort Huachuca, AZ 85613

US Army Research Office-Durham
ATTN: CRDARD-IP
Box CM, Duke Station
Durham, NC 27706

W26P8H
Contracting Officer's Representative
Night Vision Laboratory
Fort Belvoir, VA 22060
ATTN: DRSEL-NV-FIR
      Dr. Edward J. Sharp
      (20 copies/1 original)

Aerojet
Electro System Company
ATTN: P. C. Wang
1100 W. Hollyvale Street
Azusa, CA 91702

Arthur D. Little Incorporated
Acron Park
ATTN: Jacques M. Steininger
Cambridge, MA 02140

Barnes Engineering
ATTN: Dr. W. Rolls
30 Commerce Road
Stamford, CT 06902

Battelle Memorial Institute Library
505 King Avenue
Columbus, OH 43201

Cincinnati Electronics Corporation
ATTN: Dr. Vernon Lambert
2630 Glendale-Milford Road
Cincinnati, OH 45241

Electro-Optical Systems, Inc.
Solid State Department
ATTN: Dr. P.J.A. Zoutendyk
300 N. Halstead Street
Pasadena, CA 91107

Fairchild Company
Charge Coupled Device Department
ATTN: Dr. R. H. Dyck
Palo Alto, CA 94304

Ford Motor Company
Scientific Research Staff
ATTN: Dr. H. Holloway
PO Box 2053
Dearborn, MI 48121

General Dynamics
ATTN: Dr. Ester Krikorian
Mission Blvd.
Pomona, CA 91766

Honeywell Inc.
Aerospace & Defense Group
Infrared Detector Group
ATTN: George D. Anderson
1611 North Kent Street
Arlington, VA 22209

Hughes Research Laboratories
ATTN: Lloyd DeVaux
3011 Malibu Canyon Road
Malibu, CA 90265

RCA Laboratories
ATTN: R. L. Foley
Princenton, N.J. 08540

Lincoln Laboratory
Massachusetts Institute of Tech.
ATTN: Dr. I Melngailis
Lexington, MA 02173

Perkin-Elmer Corporation
Associate Director of Research
ATTN: Dr. David A. Huchital
Norwalk, CT 06852

Aeronutronics Ford Corporation
Ford Road
ATTN: Mr. Sutton
Newport Beach, CA 92663

Rockwell International Corporation
Autonetics Division
ATTN: Dr. G. Hoover or
      Dr. R. C. Geiss
PO Box 4192
3370 Miraloma Avenue
Anaheim, CA 92803

Rockwell International Corporation
Science Center
ATTN: Library (H.M. Coogan)
1049 Camino Dos Rios
Thousand Oaks, CA 91360

Commander
HQ MASTER
Technical Information Center
ATTN: Mrs. Ruth Reynolds
Fort Hood, TX 76544

USA Security Agency
ATTN: IARD
Arlington Hall Station
Arlington, VA 22212

Commander
US Army Missile Command
ATTN: AMSMI-RE (Mr. Pittman)
Redstone Arsenal, AL 35809

Commander
US Army Systems Analysis Agency
ATTN: (Mr. A. Reid)
      AMXSY-T
Aberdeen Proving Ground, MD 21005

NASA Scientific & Tech Info Facility
ATTN:  Acquisitions Branch (S-AK/DL)
P.O. Box 33
College Park, MD   20740

Chief
Ofc of Missile Electronic Warfare
Electronic Warfare Lab, ECOM
White Sands Missile Range, NM   88002

Director
Defense Advanced Research
  Projects Agency
1400 Wilson Blvd
ATTN:  Dr. R. Reynolds
Arlington, VA   22209
     (3 copies)

Naval Postgraduate School
ATTN:  Dr. F. Tao (52-TV)
Monterey, CA   93940

USNADC
ATTN:  Dr. M. Hess
Code 202149
Warminster, PA   18974

Institute of Defense Analyses
ATTN:  Dr. A.D. Schnitzler
400 Army-Navy Drive
Arlington, VA   22202

Infrared Information and
  Analysis Center
P.O. Box 618
Ann Arbor, MI   48107

Advisory Group on Electron Devices
201 Varick Street
9th Floor
New York, N.Y.   10014

Commander
U.S. Army Electronics Command
ATTN:  DRSEL-MS-TI
Fort Monmouth, N.J.   07703

Commander
U.S. Army Electronics Command
ATTN:  DRSEL-PL-ST
Fort Monmouth, N.J.   07703

Aeronutronics Ford Corporation
Aeronutronic Division
ATTN:  Mr. J. Roschen
Ford Road
Newport Beach, CA   92663

Honeywell Corporate Research Center
ATTN:  Dr. D. Long  C-1300
10701 Lyndale Ave. South
Bloomington, NM   55420

Honeywell Incorporated
ATTN:  Dr. N. Reine
2 Forbes Road
Lexington, MA   02173

Texas Instruments Incorporated
Central Research Laboratories
ATTN:  Dr. Chapman
P.O. Box 5936
13500 North Central Expressway
Dallas, TX   75222

S. Campana
Code AEYE
Naval Air Development Center
Warminster, PA   18974

K.J. Ando
Jet Propulsion Laboratory
California Institute of Technology
4800 Oak Grove Drive
Mail Stop 168-222
Pasadena, CA   91103

D.F. Barbe
Code 5214
Naval Research Laboratory
Washington, D.C.   20390

R.A. Belt
USAF Avionics Laboratory
AFAL/TEO-3, Bldg 620
Wright-Patterson Air Force Base, OH

L.W. Sumney
Code 0335
Naval Electronics System Command
Washington, D.C.

General Electric Company
ATTN:  Mr. David Schmidt
7777 Leesburg Pike
Falls Church, VA   22043

Hughes Aircraft Company
Aerospace Group
ATTN: Dr. K. Nummedall
Bldg 5, Mail Station B 169
Culver City, CA 90230

Raytheon Company
Special Micro-Wave Devices
  Operation
Infrared and Optical Research
  Laboratory
ATTN: Dr. P. Debye
130 Second Avenue
Waltham, MA 02154

Westinghouse Electric Corporation
Research & Development Center
ATTN: Dr. H.C. Nathanson
Pittsburgh, PA 15235

Rockwell International
Autonetics Division
ATTN: R. Aquilera
Anaheim, CA 92803

*Stanley Sobieski*
Code 672
Goddard Space Flight Center
Greenbelt, MD 20771

Technology Associates
ATTN: Dr. O. Trapp
51 Hillbrook Drive
Portola Valley, CA 94025

Air Force Materials Laboratory
ATTN: Robert Spry
LPO Wright-Patterson
Air Force Base, Ohio 05433

Philips Laboratories
345 Scarborough Road
Briarcliff Manor, N.Y. 10510